Research Article

Acknowledgments

We thank Dr. Charles Rice, Rockefeller University, New York, for providing replicon constructs and Huh-7.5 cells. We also thank Dr. R. Bartenschlager for providing JFH-Luc construct. This work was supported, in part, by NIH grants DK066950, CA109733, CA95490, CA35711, AA08169, P20 RR15578 and DK28614. J. Li was a liver scholar of American Liver Foundation.

Financial disclosure

The underlying research reported in the study was funded by the NIH Institues of Health.

Supplementary data

Supplementary data associated with this article can be found, in the online version, at doi:10.1016/j.jhep.2010.05.022.

References

[1] Kiyosawa K, Sodeyama T, Tanaka E, Gibo Y, Yoshizawa K, Nakano Y, et al. Interrelationship of blood transfusion, non-A, non-B hepatitis and hepatocellular carcinoma: analysis by detection of antibody to hepatitis C virus. Hepatology 1990;12:671–675.

[2] Saito I, Miyamura T, Ohbayashi A, Harada H, Katayama T, Kikuchi S, et al. Hepatitis C virus infection is associated with the development of hepatocellular carcinoma. Proc Natl Acad Sci USA 1990;87:6547–6549.

[3] Fukutomi T, Zhou Y, Kawai S, Eguchi H, Wands JR, Li J. Hepatitis C virus core protein stimulates hepatocyte growth: correlation with upregulation of wnt-1 expression. Hepatology 2005;41:1096–1105.

[4] Giannini C, Brechot C. Hepatitis C Virus biology. Cell Death Differ 2003;10 (Suppl. 1):S27–S38.

[5] Grakoui A, McCourt DW, Wychowski C, Feinstone SM, Rice CM. A second hepatitis C virus-encoded proteinase. Proc Natl Acad Sci USA 1993;90:10583–10587.

[6] Dumoulin FL, von dem Bussche A, Li J, Khamzina L, Wands JR, Sauerbruch T, et al. Hepatitis C virus NS2 protein inhibits gene expression from different cellular and viral promoters in hepatic and nonhepatic cell lines. Virology 2003;305:260–266.

[7] Rutkowski DT, Kaufman RJ. A trip to the ER: coping with stress. Trends Cell Biol 2004;14:20–28.

[8] Ma Y, Brewer JW, Diehl JA, Hendershot LM. Two distinct stress signaling pathways converge upon the CHOP promoter during the mammalian unfolded protein response. J Mol Biol 2002;318:1351–1365.

[9] Yoshida H, Haze K, Yanagi H, Yura T, Mori K. Identification of the cis-acting endoplasmic reticulum stress response element responsible for transcriptional induction of mammalian glucose-regulated proteins. Involvement of basic leucine zipper transcription factors. J Biol Chem 1998;273:33741–33749.

[10] Blight KJ, McKeating JA, Rice CM. Highly permissive cell lines for subgenomic and genomic hepatitis C virus RNA replication. J Virol 2002;76:13001–13014.

[11] Wakita T, Pietschmann T, Kato T, Date T, Miyamoto M, Zhao Z, et al. Production of infectious hepatitis C virus in tissue culture from a cloned viral genome. Nat Med 2005;11:791–796.

[12] Li JS, Tong SP, Wands JR. Characterization of a 120-Kilodalton pre-S-binding protein as a candidate duck hepatitis B virus receptor. J Virol 1996;70:6029–6035.

[13] Ingallinella P, Altamura S, Bianchi E, Taliani M, Ingenito R, Cortese R, et al. Potent peptide inhibitors of human hepatitis C virus NS3 protease are obtained by optimizing the cleavage products. Biochemistry 1998;37:8906–8914.

[14] Tong S, Li J, Wands JR. Interaction between duck hepatitis B virus and a 170-kilodalton cellular protein is mediated through a neutralizing epitope of the pre-S region and occurs during viral infection. J Virol 1995;69: 7106–7112.

[15] Franck N, Le Seyec J, Guguen-Guillouzo C, Erdtmann L. Hepatitis C virus NS2 protein is phosphorylated by the protein kinase CK2 and targeted for degradation to the proteasome. J Virol 2005;79:2700–2708.

[16] Liberman E, Fong YL, Selby MJ, Choo QL, Cousens L, Houghton M, et al. Activation of the grp78 and grp94 promoters by hepatitis C virus E2 envelope protein. J Virol 1999;73:3718–3722.

[17] Chan SW, Egan PA. Hepatitis C virus envelope proteins regulate CHOP via induction of the unfolded protein response. FASEB J 2005;19:1510–1512.

[18] Benali-Furet NL, Chami M, Houel L, De Giorgi F, Vernejoul F, Lagorce D, et al. Hepatitis C virus core triggers apoptosis in liver cells by inducing ER stress and ER calcium depletion. Oncogene 2005;24:4921–4933.

[19] Tardif KD, Mori K, Kaufman RJ, Siddiqui A. Hepatitis C virus suppresses the IRE1-XBP1 pathway of the unfolded protein response. J Biol Chem 2004;279:17158–17164.

[20] Tardif KD, Mori K, Siddiqui A. Hepatitis C virus subgenomic replicons induce endoplasmic reticulum stress activating an intracellular signaling pathway. J Virol 2002;76:7453–7459.

JOURNAL OF VIROLOGY, Sept. 2010, p. 9118–9127 Vol. 84, No. 18
0022-538X/10/$12.00 doi:10.1128/JVI.00402-10

A Disulfide-Bonded Dimer of the Core Protein of Hepatitis C Virus Is Important for Virus-Like Particle Production▽†

Yukihiro Kushima,[1,2] Takaji Wakita,[3] and Makoto Hijikata[1,2]*

Department of Viral Oncology, Institute for Virus Research, Kyoto University, Kyoto 606-8507, Japan[1]; Graduate School of Biostudies, Kyoto University, Kyoto 606-8507, Japan[2]; and Department of Virology II, National Institute of Infectious Diseases, Tokyo 162-8640, Japan[3]

Received 24 February 2010/Accepted 20 June 2010

Hepatitis C virus (HCV) core protein forms the nucleocapsid of the HCV particle. Although many functions of core protein have been reported, how the HCV particle is assembled is not well understood. Here we show that the nucleocapsid-like particle of HCV is composed of a disulfide-bonded core protein complex (dbc-complex). We also found that the disulfide-bonded dimer of the core protein (dbd-core) is formed at the endoplasmic reticulum (ER), where the core protein is initially produced and processed. Mutational analysis revealed that the cysteine residue at amino acid position 128 (Cys128) of the core protein, a highly conserved residue among almost all reported isolates, is responsible for dbd-core formation and virus-like particle production but has no effect on the replication of the HCV RNA genome or the several known functions of the core protein, including RNA binding ability and localization to the lipid droplet. The Cys128 mutant core protein showed a dominant negative effect in terms of HCV-like particle production. These results suggest that this disulfide bond is critical for the HCV virion. We also obtained the results that the dbc-complex in the nucleocapsid-like structure was sensitive to proteinase K but not trypsin digestion, suggesting that the capsid is built up of a tightly packed structure of the core protein, with its amino (N)-terminal arginine-rich region being concealed inside.

Hepatitis C virus (HCV) infection is a major cause of chronic hepatitis, liver cirrhosis, and hepatocellular carcinoma, affecting approximately 200 million people worldwide (13, 29, 44). Current treatment strategies, including interferon coupled with ribavirin, are not effective for all patients infected with HCV. An error-prone replication strategy allows HCV to undergo rapid mutational evolution in response to immune pressure and thus evade adaptive immune responses (10). New approaches to HCV therapy include the development of specifically targeted antiviral therapies for hepatitis C (STAT-Cs) which target such HCV proteins as the nonstructural 3/4A (NS3/4A), serine protease, and RNA-dependent RNA polymerase NS5B proteins (3). Despite the potent antiviral activities of some of these approaches, many resistant HCV strains have been reported after treatment with existing STAT-Cs (23, 48, 51). Therefore, identification of new targets that are common to all HCV strains and that are associated with low mutation rates is an area of active research.

HCV has a 9.6-kb, plus-strand RNA genome composed of a 5′ untranslated region (UTR), an open reading frame that encodes a single polyprotein of about 3,000 amino acids, and a 3′ UTR. The polyprotein is processed by host and viral proteases to produce three structural proteins (the core, envelope 1 [E1], and E2 proteins) and seven nonstructural proteins (the p7, NS2, NS3, NS4A, NS4B, NS5A, and NS5B proteins) (14, 16, 17, 22, 49). The HCV core protein is produced cotranslationally via carboxyl (C)-terminal cleavage to generate an immature core protein, 191 amino acids in length, on the endoplasmic reticulum (ER) (16). This protein consists of three predicted domains: the N-terminal hydrophilic domain (D1), the C-terminal hydrophobic domain (D2), and the tail domain (33), which serves as a signal peptide for the E1 protein. D1 includes a number of positively charged amino acids responsible for viral RNA binding (amino acids 1 to 75) (43) and the region involved in multimerization of the core protein via homotypic interactions (amino acids 36 to 91 and 82 to 102) (32, 40) (see Fig. S1 in the supplemental material). Hydrophobic D2 includes the region responsible for core protein association with lipid droplets (LDs; amino acids 125 to 144) (7, 18, 37), which accumulate in response to core protein production (1, 6).

Many functions of the core protein have been reported (13, 38, 50), yet because infectious HCV particles cannot be appropriately produced in currently available experimental systems, HCV particle assembly has not been elucidated to date. A cell culture system that reproduces the complete life cycle of HCV *in vitro* was developed by Wakita et al. using a cloned HCV genome (JFH1) (53). Using this system, the assembly of infectious HCV particles was found to occur near LDs and ER-derived LD-associated membranes (36, 47). Neither the structures nor the functions of the virus proteins involved in virus particle assembly are known, however. To elucidate this point, we have analyzed the biochemical characteristics of the proteins within the fraction containing the HCV particle and found a disulfide-bonded core protein complex (dbc-complex). We revealed that the disulfide-bonded dimer of core protein (dbd-core) was formed by a single cysteine residue at amino

* Corresponding author. Mailing address: Department of Viral Oncology, Institute for Virus Research, Kyoto University, 53 Kawaharacho Shougoin, Kyoto 606-8507, Japan. Phone: 81-75-751-4046. Fax: 81-75-751-3998. E-mail: mhijikat@virus.kyoto-u.ac.jp.

† Supplemental material for this article may be found at http://jvi.asm.org/.

▽ Published ahead of print on 30 June 2010.

acid position 128 on the ER. The roles of the disulfide bond of the core protein in virus-like particle formation are discussed in this paper.

MATERIALS AND METHODS

Cell culture. Cells of the HuH-7 and HuH-7.5 human hepatoma cell lines were grown in Dulbecco's modified Eagle's medium (Nacalai Tesque, Kyoto, Japan) supplemented with 10% fetal bovine serum, 100 U/ml nonessential amino acids (Invitrogen, Carlsbad, CA), and 100 μg/ml each penicillin and streptomycin sulfate (Invitrogen).

Antibodies. The antibodies used for immunoblotting and indirect immunofluorescence analysis were specific for core protein (antibody 32-1), FLAG M2 (Sigma-Aldrich, St. Louis, MO), c-myc (Sigma-Aldrich), NS5A protein (CL1), adipocyte differentiation-related protein (ADRP; StressGen, Victoria, British, Columbia, Canada), calnexin (Calnexin-NT; StressGen), and glyceraldehyde-3-phosphate dehydrogenase (GAPDH; Chemicon, Temecula, CA). Antibodies specific for core protein (antibody 32-1) were a gift from M. Kohara (The Tokyo Metropolitan Institute of Medical Science, Tokyo, Japan). Rabbit polyclonal anti-NS5A protein CL1 antibodies have been described previously (36).

Plasmid construction. All plasmids were generated by inserting PCR-amplified fragments into expression plasmids. The plasmids, primer sequences, templates for the PCRs, and restriction enzyme sites used to construct the plasmids are listed in Table S1 in the supplemental material. Plasmids pJFH1^{E2FL} (encoding the full-length HCV genome with the FLAG epitope in the E2 hypervariable region), pJFH1^{AAA99} (encoding a NS5A mutant of JFH1^{E2FL}, resulting in noninfectious HCV particles), pJFH1$^{PP/AA}$ (encoding a core protein mutant of JFH1^{E2FL}, which allows replication in cells but prevents HCV particle production), and pcDNA3-core^{WT} (an expression plasmid encoding the full-length core protein of JFH1) have been described previously (36). Plasmid pJ6/JFH1, which contains the full-length HCV genome encoding structural proteins from the J6 strain and nonstructural proteins from the JFH1 strain, was kindly provided by Charles M. Rice (The Rockefeller University, New York, NY).

***In vitro* transcription.** RNA for transfection was synthesized as described previously (36). In brief, plasmids carrying the HCV RNA sequence were linearized with XbaI and used as templates for *in vitro* transcription with MEGAscript T7 (Ambion, Austin, TX).

Transfection. Ten micrograms of JFH1^{E2FL}, JFH1^{C128A}, JFH1^{C184A}, JFH1$^{C128/184A}$, JFH1$^{PP/AA}$, or JFH^{AAA99} and J6/JFH1 or J6/JFH1^{AAA99} RNAs were transfected into HuH-7 and HuH-7.5 cells (1.0×10^7 cells) by electroporation (260 V, 0.95 μF) using a Gene Pulser II system (Bio-Rad, Hercules, CA). Core protein expression plasmids were transfected into HuH-7 cells using Lipofectamine LTX (Invitrogen), according to the manufacturer's protocol.

HCV particle precipitation. Culture medium from HCV RNA-transfected cells were concentrated using Amicon Ultra-15 centrifugal filters with Ultracell-100 membranes (Millipore, Billerica, MA) and mixed with sucrose solution in phosphate-buffered saline (PBS) to a final sucrose concentration of 2%. This mixture was ultracentrifuged (100,000 × *g*, 4°C for 2 h), and the HCV particles were obtained as a pellet. The pellet was then suspended in culture medium for infection experiments or PBS for immunoblot analysis.

Indirect immunofluorescence analysis. Indirect immunofluorescence analyses of HCV infection and the cellular localization of the HCV proteins were performed as described previously (36).

Protease protection assay. Concentrated culture medium from JFH1^{E2FL} RNA-transfected HuH-7 cells was fractionated using 20 to 50% sucrose density gradients, and the HCV RNA titer was measured in quantitative reverse transcription-PCRs (RT-PCRs) as described below. Fractions with high HCV RNA titers were collected, and JFH1^{E2FL} particles were obtained as a pellet after ultracentrifugation (100,000 × *g*, 4°C for 2 h). The pellet was suspended in PBS and treated with 10 μg/ml trypsin or 5 μg/ml proteinase K in the presence or absence of 1% Nonidet P-40 (NP-40) at 37°C for 15 min, unless otherwise indicated. The reaction was quenched by the addition of protease inhibitor cocktail (Nacalai Tesque), followed by SDS-PAGE under nonreducing conditions and immunoblotting specific for core protein.

Immunoblot analysis. Samples were subjected to SDS-PAGE in sample buffer (62.5 mM Tris-HCl [pH 7.8], 1% SDS, 10% glycerol) with or without 5% β-mercaptoethanol (β-ME) or 50 mM dithiothreitol (DTT) for reducing and nonreducing conditions, respectively. *N*-Ethylmaleimide (NEM; Nacalai Tesque) was added to the sample buffer to a final concentration of 5 mM for the indicated samples. Proteins were transferred to a polyvinylidene difluoride membrane and blocked in blocking buffer for 1 h at room temperature with gentle agitation. After incubation with primary antibodies overnight at 4°C, the membrane was washed three times for 5 min in washing buffer at room temperature with gentle agitation. The membrane was then incubated with horseradish peroxidase (HRP)-conjugated secondary antibodies for 1 h at room temperature. After three washes in washing buffer, proteins were detected using Western Lightning reagent (PerkinElmer, Waltham, MA) or ECL Advance (GE Healthcare, Buckinghamshire, England) and Kodak MXJB Plus medical X-ray film (Kodak, Rochester, NY) or an LAS-4000 system (Fujifilm, Tokyo, Japan).

Preparation of LDs. LDs were prepared as described previously (36).

Preparation of MMFs. Microsomal membrane fractions (MMFs) were collected as described previously (15) with some modifications. In brief, cells were collected in homogenization buffer (20 mM Tris-HCl [pH 7.8], 250 mM sucrose, and 0.1% ethanol supplemented with protease inhibitor cocktail) and homogenized on ice using 40 strokes of a Dounce homogenizer. The samples were then centrifuged at 1,000 × *g* for 10 min at 4°C. The supernatant was collected in a new tube and centrifuged again at 16,000 × *g* for 20 min at 4°C. The supernatant was further centrifuged at 100,000 × *g* for 1 h at 4°C. The MMF precipitate was homogenized in lysis buffer (1% NP-40, 0.1% SDS, 20 mM Tris-HCl [pH 8.0], 150 mM NaCl, 1 mM EDTA, and 10% glycerol supplemented with protease inhibitor cocktail) using a Dounce homogenizer.

qRT-PCR analysis. Quantitative RT-PCR (qRT-PCR) analysis for determination of the HCV RNA titer was performed as described previously (36).

ELISA specific for core protein. The core protein in culture medium was quantified using an enzyme-linked immunosorbent assay (ELISA; HCV antigen ELISA; Ortho-Clinical Diagnostics, Raritan, NJ), according to the manufacturer's protocol.

RNA-protein binding precipitation assay. Core^{WT} or core^{C128A} was translated *in vitro* from pcDNA3-core^{WT} and pcDNA3-core^{C128A}, respectively, using a TNT-coupled rabbit reticulocyte lysate system (Promega, Madison, WI), according to the manufacturer's protocol. These proteins were incubated with poly(U) agarose (Sigma) in binding buffer (50 mM HEPES (pH 7.4)–100 mM NaCl–0.1% NP-40–20 U RNase inhibitor) at 4°C for 2 h with or without RNase A. After five washes, the resin-bound core proteins were immunoblotted.

RESULTS

The HCV particle contains core protein complex formed by a disulfide bond. To analyze the core protein of the HCV particle, we first subjected the concentrated culture medium of HuH-7 cells transfected with *in vitro*-transcribed JFH1^{E2FL} RNA to ultracentrifugation. After the resulting pellet was resuspended in culture medium, we confirmed the presence of infectious HCV particles on the basis of the infectivity of HuH-7.5 cells (Fig. 1a). The infectious JFH1^{E2FL} particle-containing pellet was separated by SDS-PAGE under nonreducing conditions, and immunoblot analysis showed the presence of a core antibody-reactive protein that was approximately twice the size of the core protein (38 kDa), in addition to the expected 19-kDa core protein (Fig. 1b, lane 1). Because treatment with DTT eliminated the larger core protein antibody-reactive band while the levels of the core protein monomer increased (Fig. 1b, lanes 2 to 6), the larger protein likely represented a dbc-complex. This complex was also found in J6/JFH1-derived particles (see Fig. S2 in the supplemental material), indicating that the complex was not specific for JFH1^{E2FL}.

To determine whether the dbc-complex is a component of the HCV particle, a protease protection assay was performed using RNase-resistant HCV particles fractionated on the basis of their buoyant densities. Concentrated culture medium from HuH-7 cells transfected with *in vitro*-transcribed JFH1^{E2FL} RNA was fractionated using a 20 to 50% sucrose density gradient; and JFH1^{E2FL} particles, which were presumed to contain both infectious and noninfectious particles, were collected from fractions with high HCV RNA titers using ultracentrifugation (Fig. 2a, fractions 8 to 13). The core protein from the collected fractions was analyzed by immunoblotting after SDS-

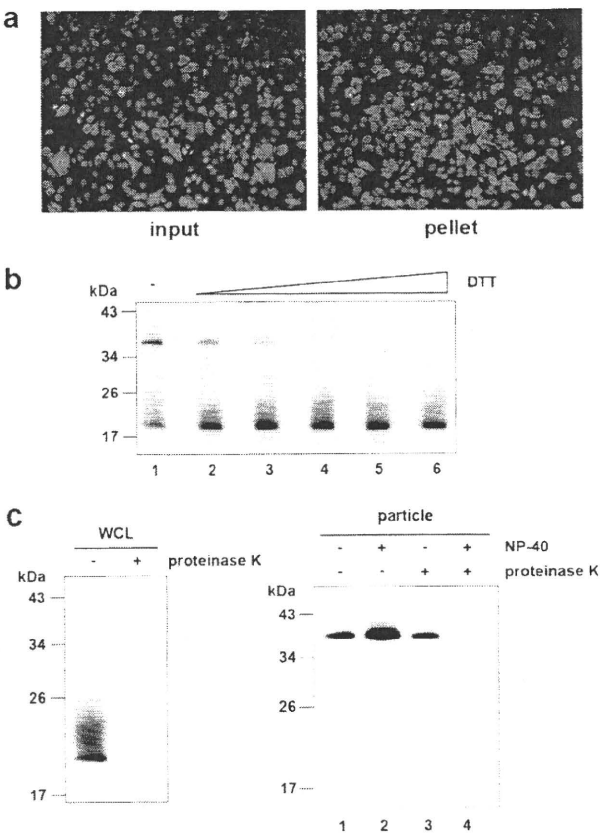

FIG. 1. The HCV-like particle consists of a core complex formed by a disulfide bond. (a) The infectivity of the pellet fraction collected from concentrated culture medium from $JFH1^{E2FL}$ RNA-transfected HuH-7 cells was analyzed as described in Materials and Methods. Input indicates the same volume of concentrated culture medium used to pellet the virus-like particles. (b) Immunoblot analysis of the core protein in pellets containing $JFH1^{E2FL}$ virus particles treated with various levels of DTT (lanes 1, 2, 3, 4, 5, and 6, 0, 1.56, 3.13, 6.25, 12.5, and 25 mM DTT, respectively). (c) Immunoblot analysis of the core protein in $JFH1^{E2FL}$ particles collected from sucrose density gradient fractions with high HCV RNA titers (particle) (Fig. 2a, fractions 8 to 13) and treated with 5 μg/ml proteinase K at 37°C for 15 min in the presence or absence of 1% NP-40 (right panel). As a positive control, WCL prepared from $JFH1^{E2FL}$ RNA-transfected HuH-7 cells in lysis buffer was treated with 5 μg/ml proteinase K at 37°C for 15 min (left panel). Data are representative of three independent experiments.

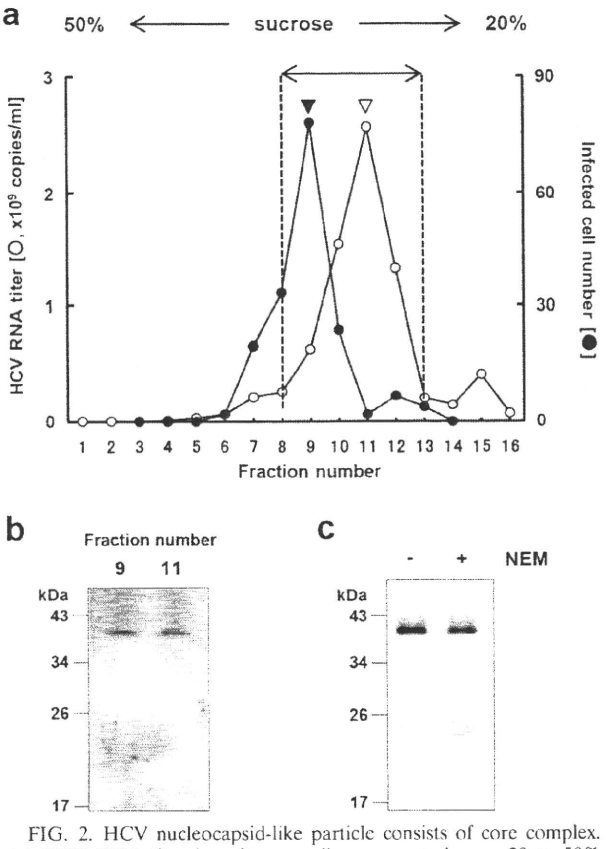

FIG. 2. HCV nucleocapsid-like particle consists of core complex. (a) HCV RNA titer in culture medium separated on a 20 to 50% sucrose density gradient. Concentrated culture medium from $JFH1^{E2FL}$ RNA-transfected HuH-7 cells were treated with RNase and separated on a 20 to 50% sucrose density gradient. Fractions 1 to 16 were obtained from the bottom to the top of the tube, respectively. The HCV RNA titer and infectivity of each fraction were analyzed by real-time qRT-PCR (for fractions 1 to 16) and counting the number of cells infected with HCV-like particle detected by immunofluorescence (for fractions 3 to 14), respectively, as described in Materials and Methods. In brief, each fraction was diluted with 1× PBS and HCV-like particles were collected by ultracentrifugation, and then the pellets were suspended in culture medium and used for infection. (b) HCV-like particle collected from the infectious HCV peak (from panel a, filled arrowhead) and the HCV RNA peak (from panel a, open arrowhead) were collected by ultracentrifugation, subjected to nonreducing SDS-PAGE, and detected by immunoblotting against the core protein. (c) HCV-like particles collected from fractions 8 to 13 (a) were subjected to nonreducing SDS-PAGE in the presence (lane +) or absence (lane −) of 5 mM NEM and analyzed by immunoblotting against the core protein. Data are representative of two (a, infectivity of fractions) or three independent experiments.

PAGE under nonreducing conditions and showed only the dbc-complex (Fig. 1c, right panel).

To examine whether the complex contributes to the infectivity of the particles, we analyzed the dbc-complex in the fractions containing infectious and noninfectious HCV particles (fractions 9 and 11 of Fig. 2a, filled and open arrowheads, respectively). Both the infectious and noninfectious HCV particle-containing fractions contained the dbc-complex (Fig. 2b). To confirm this further, a pellet containing particles of mutant $JFH1^{AAA99}$—a mutant of $JFH1^{E2FL}$ that primarily produces noninfectious particles (36)—was analyzed in a similar manner. These dbc-complexes were found in pelleted particles of both $JFH1^{AAA99}$ and $J6/JFH1^{AAA99}$, which was a mutant J6/JFH1 with a similar substitution to $JFH1^{AAA99}$ (see Fig. S2 in the supplemental material). These results indicated that the dbc-complex was present in both the infectious and noninfectious HCV-like particles.

The core protein monomer observed in the pellet samples (Fig. 1b) may be from the secreted core protein or the debris of apoptotic cells, because the core protein is known to be secreted from cells expressing this protein under particular conditions (42) and strain JFH1 is known to cause apoptosis (45). The dbc-complex-specific signals in the HCV particles seem to be increased in the NP-40-treated samples for some

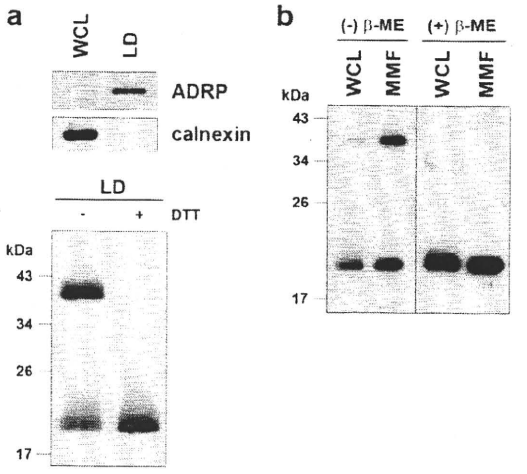

FIG. 3. The core complex is formed at the LD and ER. (a) The LD fraction and WCL were collected from JFH1^{E2FL} RNA-transfected HuH-7 cells on day 5 posttransfection. (upper panel) Immunoblot analysis of the LD marker ADRP and the ER marker calnexin in the LD fraction; (lower panel) immunoblot analysis of the core protein in the LD fraction treated or not treated with 50 mM DTT. (b) Immunoblot analysis of the core protein in the MMF and WCL collected from JFH1^{E2FL}-producing HuH-7 cells on day 5 posttransfection in the presence or absence of 5% β-ME. Data are representative of those from three independent experiments.

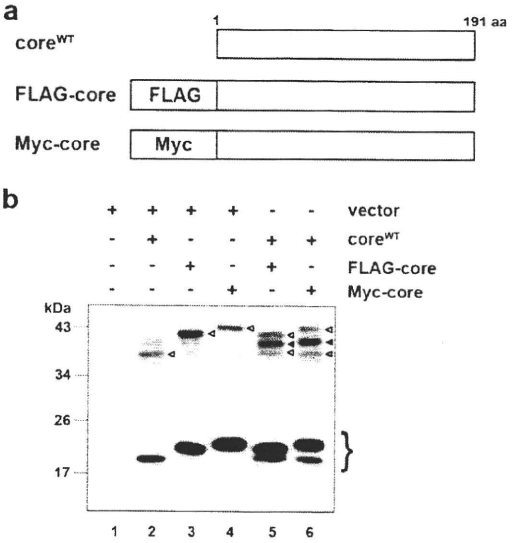

FIG. 4. The core complex consists of a core dimer. (a) Schematic of wild-type, FLAG-tagged (FLAG-core), and Myc-tagged (Myc-core) core proteins. (b) Immunoblot analysis of the core protein in the MMF collected from HuH-7 cells transfected with combinations of pcDNA3 (vector) and/or core expression plasmids (e.g., encoding core^{WT}, FLAG-core, and Myc-core), as indicated. The experiment was performed under nonreducing conditions. The lower bands represent core monomer (marked on the right with a brace). White arrowheads, bands corresponding to dbd-core; black arrowheads, positions of the intermediately sized core complex formed by core^{WT} and the tagged core. Data are representative of those from three independent experiments.

unknown reason (Fig. 1c, lanes 1 and 2). Although the intermolecular disulfide bond is known to be artificially formed in denaturing SDS-PAGE in the absence of reducing agents, the dbc-complex was still observed even in the presence of NEM, which is the alkylating agent for free sulfhydryls, during sample preparation (Fig. 2c), indicating that the dbc-complex was naturally present in the virus-like particles.

The HCV nucleocapsid is covered with lipid membranes and E1 and E2 proteins, making it resistant to proteases. As expected, in the absence of NP-40, the dbc-complex was resistant to proteinase K (Fig. 1c, lane 3), whereas proteinase K was able to digest core protein in whole-cell lysates (WCLs) collected from JFH1^{E2FL}-transfected HuH-7 cells (Fig. 1c, left panel). Disrupting the envelope structure with NP-40 made the dbc-complex susceptible to proteinase K treatment (Fig. 1c, lane 4), indicating that the dbc-complex was indeed a component of the HCV particle.

The dbc-complex forms on the ER. To investigate the subcellular site at which the dbc-complex forms, LDs and MMFs from JFH1^{E2FL} replicating HuH-7 cells were analyzed by immunoblotting. We first analyzed the dbc-complex in LDs, because LDs are involved in infectious HCV particle formation (36, 47). The purity of the LD fraction was determined using immunoblot analysis of calnexin and ADRP, ER and LD marker proteins, respectively (Fig. 3a, upper panel). The core protein was then analyzed in the LD fraction. As shown in Fig. 3a (lower panel), the dbc-complex was observed in the LD fraction from JFH1^{E2FL} RNA-transfected HuH-7 cells. We next analyzed the core protein in the ER-containing MMF, because the core protein is first translated and processed on the ER (16). As shown in Fig. 3b, the dbc-complex was observed in the MMF from JFH1^{E2FL} RNA-transfected HuH-7 cells. These results suggest that the dbc-complex is first formed at the ER. To assess the possibility that dbc-complex-containing HCV particles were also assembled on the ER, the sensitivity of the dbc-complex to protease treatment was analyzed. The dbc-complex in the MMF was susceptible to protease treatment in the absence of NP-40, indicating that the dbc-complex on the ER was not yet part of a HCV particle (data not shown).

dbc-complex is most likely a disulfide-bonded dimer form of the core. In order to examine whether the core protein itself has the potential to form a dbc-complex, we analyzed the dbc-complex formation of the full-length wild-type core protein (core^{WT}) expressed from pcDNA3-core^{WT} (36), the expression plasmid encoding the 191-amino-acid full-length core protein of JFH1 strain. We used this expression plasmid because the core protein from this plasmid was likely to be processed correctly enough to produce infectious HCV particles when it was cotransfected with the RNA of JFH1^{dc3}, which is a core protein deletion mutant of JFH1 (36). As a result, the dbc-complex formation was observed from the MMF of core^{WT}-expressing cells both in the absence and in the presence of NEM (Fig. 4b; lane 2 and data not shown, respectively). We next investigated the effect of the amino acid region of E1 on the production of the dbc-complex, because it has been reported that the efficient processing of core protein is dependent on the presence of some E1 sequence to ensure the insertion of the signal sequence for E1 in the translocon/membrane machinery (34). The dbc-complex was also observed

when the core protein was expressed from pcDNA3-C-E1/25, which encodes the full-length core protein followed by the N-terminal 25-amino-acid sequence of E1 to ensure that the core protein is processed properly (see Fig. S3a in the supplemental material). These data showed that the dbc-complex was formed by expression of the core protein only in the cells.

Next, we examined the structural components of the dbc-complex. Because the dbc-complex was twice the size of the core protein monomer, it was likely dbd-core. So, we investigated whether the core protein molecules with different tags were able to form the dbd-core. We first generated expression plasmids encoding core protein with the N-terminal FLAG and Myc tags (pcDNA3-FLAG-core and pcDNA3-Myc-core, respectively; Fig. 4a). The tagged core proteins were expressed or coexpressed with $core^{WT}$ in HuH-7 cells, and the MMF was analyzed by immunoblotting. The FLAG or Myc tag shifted the positions of the monomer and the complex bands (Fig. 4b, lanes 3 and 4) compared with the position of $core^{WT}$ (Fig. 4b, lane 2). When $core^{WT}$ was coexpressed with FLAG-core or Myc-core, the core protein complex of an intermediate size was observed, in addition to the bands obtained when the constructs were independently expressed (Fig. 4b, lanes 5 and 6, filled arrowheads); the intermediate-sized band disappeared after treatment with β-ME (see Fig. S3b, lanes 11 and 12, filled arrows, in the supplemental material), indicating that $core^{WT}$ and tagged core protein formed a heteromeric disulfide-bonded dimer. These results demonstrated that the dbc-complex on the ER is a dbd-core. Although we tried to detect the hetero- or homodimer consisting of the tagged core protein by using anti-FLAG or anti-Myc antibodies, these dimers were not detected, possibly because of the lower levels of sensitivity and specificity of the antibodies compared to those of the anti-core protein antibody that we used, especially against epitopes in the dbd-core. The results presented above, coupled with the similarities of the molecular sizes and sensitivities to β-ME and DTT, suggested that the dbc-complex in the HCV particle is most likely a dbd-core.

Core protein Cys128 mediates dbd-core formation. Our results showed that core protein from $JFH1^{E2FL}$ forms a disulfide-bonded dimer on the ER. A search for cysteine residues in the $JFH1^{E2FL}$ core protein identified amino acid positions 128 (Cys128) and 184 (Cys184) (see Fig. S1 in the supplemental material). These residues are highly conserved in core proteins from the approximately 2,000 reported HCV strains (HCVdb, http://www.hcvdb.org/, Hepatitis C Virus Database; http://s2as02.genes.nig.ac.jp/). To determine which cysteine residue mediated disulfide bond formation, we generated point mutations in $JFH1^{E2FL}$ that replaced Cys128 and/or Cys184 with alanine (Ala) (C128A, C184A, and C128/184A in $JFH1^{C128A}$, $JFH1^{C184A}$, and $JFH1^{C128/184A}$, respectively; Fig. 5a). As shown in Fig. 5b, the core proteins from $JFH1^{C128A}$ and $JFH1^{C128/184A}$ failed to form a dbd-core under nonreducing condition, whereas the core protein from $JFH1^{C184A}$ formed the dimer, indicating that Cys128 was the residue responsible. Similar results were observed when Cys was replaced by serine (Ser) instead of Ala (see Fig. S5c in the supplemental material). Recently, Majeau et al. reported that the core protein of the J6/JFH1 strain with Cys128 replacements by Ala or Ser were unstable in both *Pichia pastoris* and human hepatoma cell line HuH-7.5 (31), although we did not detect any noticeable degradation of the mutant core proteins of strain JFH1 (Fig. 5b; see also Fig. S5c in the supplemental material). This difference may have resulted from the difference in sample preparation methods, as we used the full-length genome of $JFH1^{E2FL}$ strain bearing the strain JFH1 core protein and HuH-7 cells instead of a core protein-expressing plasmid for the J6 strain and HuH-7.5 cells.

To exclude the possibility that mutation of Cys128 inhibited dbd-core formation by creating a conformational change, T127A and G129A core protein mutants ($JFH1^{T127A}$ and $JHF1^{G129A}$, respectively) were created and examined for their effects on dbd-core formation and infectious virus particle production. These mutants formed dbd-core, and infectious HCV particles were detected in the culture medium (see Fig. S4a to c in the supplemental material), supporting an essential role for Cys128 in dbd-core and particle formation.

dbd-core contributes to HCV particle production. To examine the functional roles of dbd-core, infectious HCV particle production, HCV replication efficiency, colocalization of the core protein and LDs, and RNA binding of mutant and wild-type ($JFH1^{E2FL}$) core protein were evaluated. Culture medium from HuH-7 cells transfected with $JFH1^{C128A}$ or $JFH1^{C128/184A}$ RNA contained significantly fewer infectious HCV particles compared with the numbers obtained with $JFH1^{E2FL}$ or $JFH1^{C184A}$ RNA (Fig. 5c). We also found significant decreases in the levels of HCV RNA and core protein in the culture medium of HuH-7 cells transfected with $JFH1^{C128A}$ or $JFH1^{C128/184A}$ RNA (Fig. 5d and e). Similar results were observed with J6/JFH1 C128A or the C128/184A mutant strain (data not shown). To investigate whether these results were due to suppressed HCV replication, the HCV RNA and protein levels in cells transfected with mutant RNA were analyzed using qRT-PCR and immunoblot analyses, respectively. Compared with the results obtained with $JFH1^{E2FL}$, no significant changes in the cellular HCV RNA titer at days 1, 3, and 5 posttransfection or in the expression of HCV nonstructural protein NS5A were observed (Fig. 6a and b). This indicated that substitution of Cys128 did not significantly affect HCV RNA genome replication or viral protein production, demonstrating that the dbd-core functions during HCV particle production rather than HCV genome replication. Similar results were observed using RNA of JFH1 mutant strain $JFH1^{C128S}$, in which the cysteine at position 128 was replaced by Ser instead of Ala (see Fig. S5a, b, and d in the supplemental material).

The subcellular localizations of the core protein and NS5A protein in HuH-7 cells transfected with HCV RNA were investigated using indirect immunofluorescence and confocal microscopy, because recruiting HCV proteins to LDs is an important step in infectious HCV particle production (36, 47) and core trafficking to LDs is dependent on signal peptide peptidase (SPP)-mediated cleavage of the tail region (34, 41). $JFH1^{C128A}$ mutant core protein and NS5A protein were efficiently trafficked to LDs, as was observed with wild-type $JHF1^{E2FL}$ (Fig. 6c), suggesting that SPP cleavage and core protein maturation were not affected by the C128A mutation. Similar results were obtained with the core proteins derived from $JFH1^{C184A}$ and $JFH1^{C128/184A}$ (see Fig. S6 in the supplemental material) and also Ser mutant $JFH1^{C128S}$ (see Fig. 5e in the supplemental material).

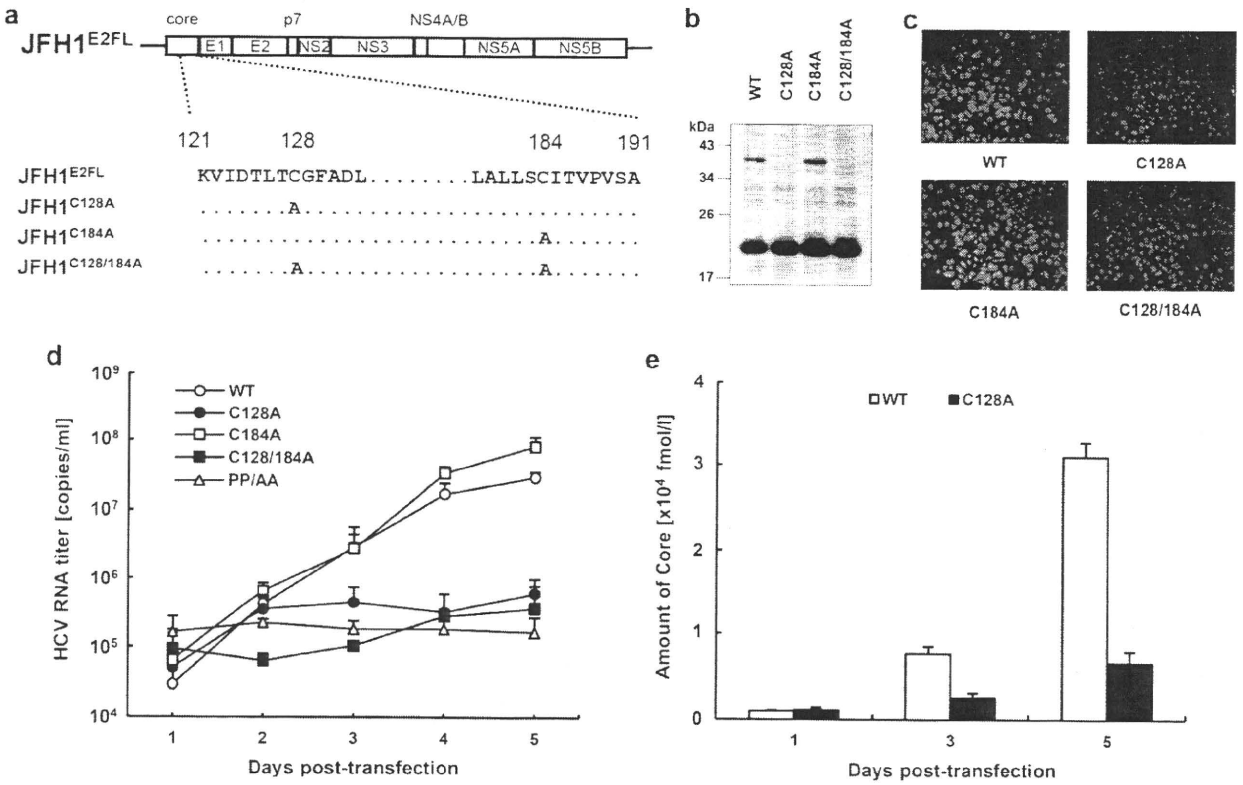

FIG. 5. The core dimer is formed via a bond between cysteine residues at amino acid position 128. (a) Site-directed mutagenesis of $JFH1^{E2FL}$. (b) Immunoblot analysis of the core protein in MMFs collected from HuH-7 cells under nonreducing conditions 3 days post-transfection with $JFH1^{E2FL}$ (WT), $JFH1^{C128A}$ (C128A), $JFH1^{C184A}$ (C184A), or $JFH1^{C128/184A}$ (C128/184A) RNA. (c) Infectivity of culture medium collected and concentrated on day 5 posttransfection from HuH-7 cells transfected with WT, C128A, C184A, or C128/184A RNA. (d) Real-time qRT-PCR analysis of HCV RNA titers in culture medium collected at the indicated time points from HuH-7 cells transfected with WT, C128A, C184A, C128/184A, or PP/AA ($JFH1^{PP/AA}$) RNA. (e) ELISAs of core protein levels in culture medium collected at the indicated time points from HuH-7 cells transfected with WT or C128A RNA. Data are representative of those from three independent experiments (b and c) or are the means ± standard deviations from three independent experiments (d and e).

Because HCV core protein can bind to RNA, including the HCV genome, during viral particle assembly (43), we analyzed RNA binding by the core protein using *in vitro*-translated $core^{C128A}$, $core^{WT}$, and poly(U) agarose resin. $Core^{C128A}$ and $core^{WT}$ bound similarly to the poly(U) resin (Fig. 6d).

dbd-core is important for HCV particle assembly. The mutational analysis of the core protein indicated that $core^{C128A}$ and $core^{WT}$ similarly localize to LDs, recruit NS proteins to the LD, and bind to RNA. Moreover, this mutation did not markedly affect HCV genome replication. How does $core^{C128A}$ affect the production of HCV particles? An important function of the core protein is multimerization, which is followed by capsid construction and packaging of the RNA genome in the viral particles. We therefore determined whether $core^{C128A}$ had a dominant negative effect on virus-like particle production. Wild-type $JFH1^{E2FL}$ RNA and different amounts of $JFH1^{C128A}$ RNA were cotransfected into HuH-7 cells, and the HCV RNA titer and infectivity of the virus-like particles in the culture medium were analyzed. As expected, the HCV RNA titer in the cells increased with higher levels of transfected RNA (see Fig. S7a in the supplemental material). In contrast, the HCV RNA titer and infectivity in the culture medium decreased in a $JFH1^{C128A}$ RNA dose-dependent manner when this mutant RNA was cotransfected with wild-type RNA (Fig. 7a, b). This suppressive effect was not observed when either wild-type RNA or core deletion mutant $JFH1^{dc3}$ RNA was used instead of mutant RNA in a similar experiment (see Fig. S7b to e in the supplemental material), indicating that higher levels of HCV RNA alone did not inhibit HCV particle production. Thus, $core^{C128A}$ had a dominant negative effect on HCV particle production. Together, these results suggest that dbd-core is involved in the assembly of HCV particles.

The nucleocapsid-like particle of HCV was resistant to trypsin treatment. To further investigate the structure of the HCV nucleocapsid-like particle most likely formed by dbd-core, we examined the sensitivity of the particle to trypsin, which cleaves polypeptides at the C-terminal end of basic residues. Whereas trypsin digested the core protein in the whole-cell lysates (Fig. 8a, left panel), dbd-core from buoyant density-fractionated $JFH1^{E2FL}$ particles was resistant to digestion, despite NP-40 treatment (Fig. 8a, right panel), although it was sensitive to proteinase K, which has a broad specificity (Fig. 1c). The N-terminal hydrophilic domain of the core protein (from residues 6 to 121) contains a number of trypsin cleavage sites (25 sites

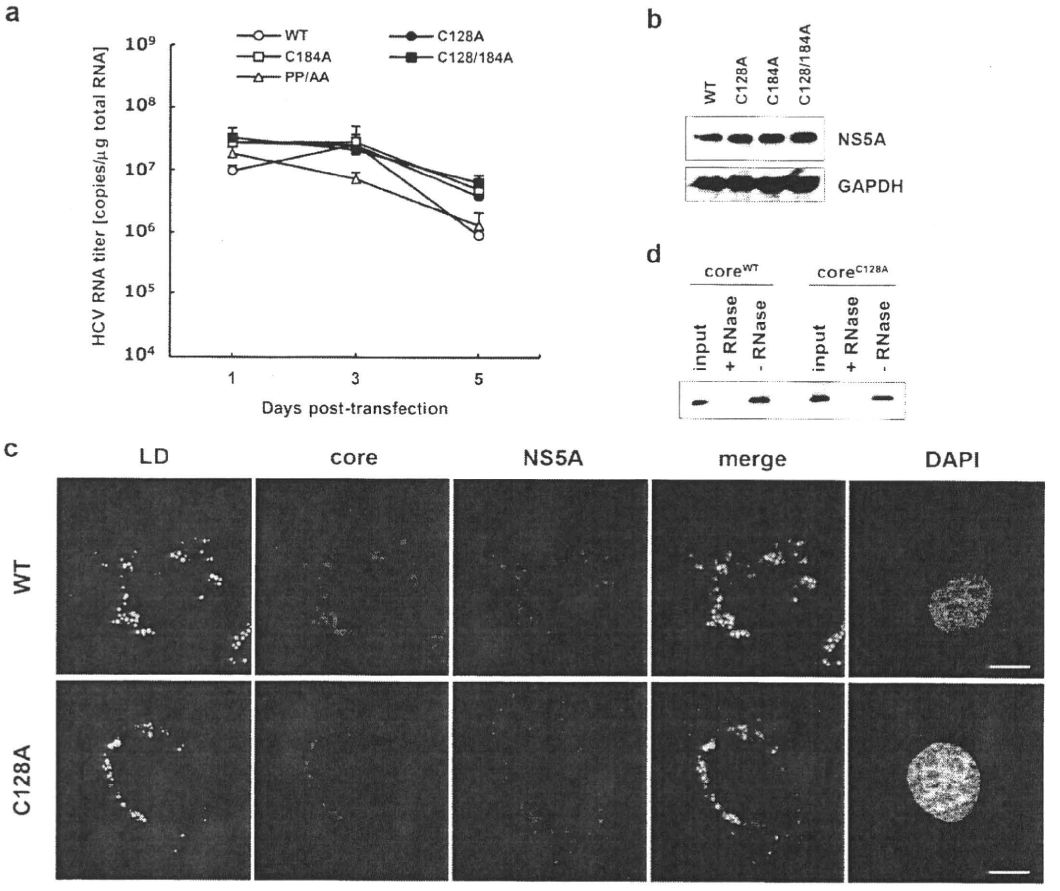

FIG. 6. Site-directed mutagenesis has no effect on HCV replication. (a) Real-time qRT-PCR analysis of the HCV RNA titer using total cellular RNA collected at the indicated time points from cells transfected with JFH1^{E2FL} (WT), JFH1^{C128A} (C128A), JFH1^{C184A} (C184A), JFH1$^{C128/184A}$ (C128/184A), or JFH1$^{PP/AA}$ (PP/AA) RNA. (b) Immunoblot analysis of NS5A protein and GAPDH in whole-cell lysate collected from cells transfected with WT, C128A, C184A, or C128/184A RNA at day 3 posttransfection. (c) Confocal microscopy of the subcellular localization of the LD (green), core (blue), NS5A protein (red), and nucleus (4′,6-diamidino-2-phenylindole [DAPI]) (gray) in WT and C128A replicating cells on day 3 posttransfection. Bars, 10 μm. (d) An RNA-protein binding precipitation assay was performed with *in vitro*-translated core^{WT} and core^{C128A} using poly(U) agarose as the resin. +RNase and −RNase, samples with and without RNase treatment, respectively, as described in Materials and Methods. Input indicates that 1/40 of the amount of translated product was used in this assay. Data represent the means ± standard deviations from three independent experiments (a) or are representative of those from three independent experiments (b to d).

in strain JHF1) (see Fig. S1 in the supplemental material), suggesting that the N-terminal domain faces inward and/or that the conformation prevents protease access. To address this idea, buoyant density-fractionated JFH1^{E2FL} particles were treated with trypsin under stricter conditions in the presence of NP-40. Cleavage of dbd-core by various levels of trypsin correlated with the appearance of a shorter molecule (Fig. 8b, white arrowhead). The shorter molecule was presumed to be partially digested dbd-core with an intact N-terminal region because it was recognized by anti-core protein antibodies, which bind to an epitope located from amino acids 20 to 40 of the core protein (M. Kohara, The Tokyo Metropolitan Institute of Medical Science, personal communication). These results suggest that dbd-core is assembled into the nucleocapsid-like particle such that most of the N-terminal domain is inside.

DISCUSSION

In the present study, we have shown that the nucleocapsid-like particle of HCV most likely contains a dimer of core protein that is stabilized by a disulfide bond. Mutational analysis revealed that Cys128 forms a disulfide bond between core monomers. Several reports have shown that disulfide bonds in the capsid proteins of some viruses are involved in virus particle assembly and stabilization of the viral capsid structure (4, 21, 27, 28, 57); these viruses are characterized by icosahedral nucleocapsids. Because, like these viruses, the HCV virion is spherical (2, 20), it has been suggested that HCV may contain a nucleocapsid with a similar structure (20). We found the dbc-complex, which is most likely to be the dbd-core in JFH1^{E2FL} virus-like particles (Fig. 1c and 8a). The dbd-core in the capsid structure was digested by proteinase K but not

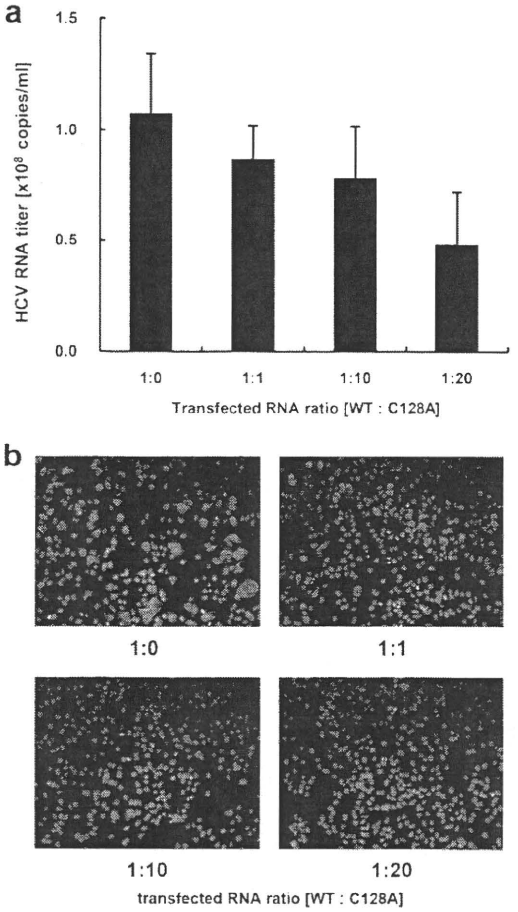

FIG. 7. JFH1^{C128A} core inhibits JFH1^{E2FL} particle assembly. A competitive inhibitory assay was performed with JFH1^{E2FL} (WT) and JFH1^{C128A} (C128A). (a) Real-time qRT-PCR analysis of the HCV RNA titer in HuH-7 cell culture medium 3 days after the cells were transfected with the indicated ratio of WT and C128A RNA. (b) The infectivity of culture medium collected from HuH-7 cells that had been transfected with the indicated ratio of WT and C128A RNA was analyzed as described in Materials and Methods. Data represent the means ± standard deviations from three independent experiments (a) or are representative of those from three independent experiments (b).

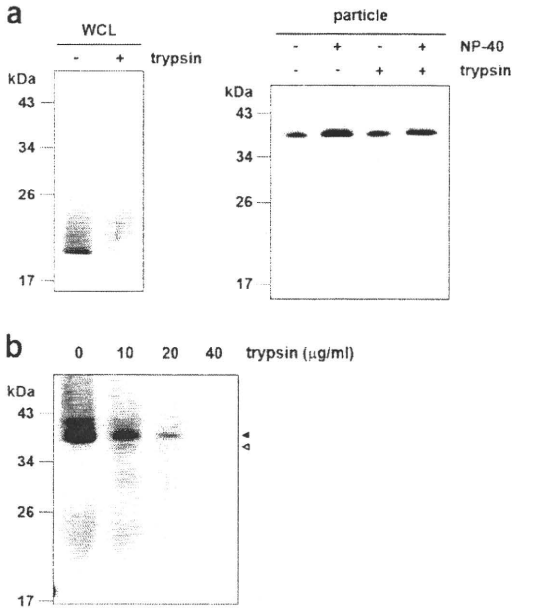

FIG. 8. The nucleocapsid-like particle of JFH1^{E2FL} is assembled with the C-terminal region of the core protein on the outer surface. (a) Immunoblot analysis of the core protein in JFH1^{E2FL} particles collected from sucrose density gradient fractions with high HCV RNA titers (particle) (Fig. 2a, fractions 8 to 13). The fractions were treated with 10 μg/ml trypsin at 37°C for 15 min in the presence or absence of 1% NP-40 (right panel). As a positive control, WCL prepared from JFH1^{E2FL} RNA-transfected HuH-7 cells in lysis buffer was treated with 10 μg/ml trypsin at 37°C for 15 min (left panel). (b) Immunoblot analysis of the core protein in JFH1^{E2FL} particles collected from sucrose density gradient fractions with high HCV RNA titers (Fig. 2a, fractions 8 to 13). The fractions were treated with the indicated concentrations of trypsin at 37°C for 10 min in the presence of 1% NP-40. Open and filled arrows indicate the positions of dbd-core and the trypsin-digested fragment, respectively. Data are representative of those from three independent experiments.

trypsin in the presence of NP-40 (Fig. 1c and 8a, lane 4). The resistance to trypsin suggested a tight conformation for dbd-core in the capsid and no exposed trypsin cleavage sites. The truncated form of dbd-core that was observed under certain trypsin treatment conditions likely resulted from cleavage in the C-terminal portion of the protein (e.g., arginine residues at positions 149 and 156) (see Fig. S1 in the supplemental material), although it is possible that the truncation of dbd-core was due to nonspecific cleavage by trypsin. These results imply that dbd-core is configured such that the N- and C-terminal ends are located at the inner and outer surfaces of the capsid, respectively. Because the N-terminal region of the core protein includes the RNA binding domain (43), the HCV RNA genome likely interacts with the core protein as it is packed in the nucleocapsid. On the other hand, the C-terminal hydrophobic domain probably faces the lipid membranes to form the envelope structure. Only part of the N-terminal hydrophilic region of the core protein has been structurally examined using X-ray crystal structural analysis (35) and structural bioinformatics and nuclear magnetic resonance analysis (11). Although the C-terminal half of the core protein has been structurally investigated by the use of bioinformatics (8), the three-dimensional structure containing the Cys128 residue is unknown. Thus, determination of the structure of the core protein in the nucleocapsid containing the Cys128 residue should be required for understanding the whole structure of this protein in the virus particles.

Because cotransfection of JFH1^{C128A} RNA with wild-type JFH1^{E2FL} RNA inhibited particle production in a mutant RNA dose-dependent manner (Fig. 7a and b), the C128A core variant clearly inhibited HCV particle formation by wild-type core protein. Cys128 was also previously reported to be a residue included in the region important for the production of infectious HCV (39). This residue is located near the N-terminal end of the hydrophobic region of the core (amino acids 122 to 177) and belongs to the hydrophilic side of an amphipathic helix expected to interact in the plane of the membrane interface (7). Therefore, it is possible to think that dbd-core

formation via Cys128 can stabilize the interaction between the core protein and the membranes. The N-terminal half of the core protein (amino acids 1 to 124) reportedly assembles into nucleocapsid-like particles in the presence of the 5′ UTR from HCV RNA (24), suggesting that some nucleocapsid-like particles may assemble via only homotypic interactions from the core protein. In addition to weak homotypic interactions, the HCV core protein forms a disulfide bond to stabilize the capsid structure, thus making dbd-core indispensable in the stable virus-like particle. We observed that culture medium from JFH1^{C128A}- or JFH1^{C128S}-transfected cells included slight infectivity (Fig. 5c; see also Fig. S5d in the supplemental material). This made us speculate that this mutant may produce some infective particle-like structure formed by a homotypic interaction of the core. Such a slight infectivity may have reflected the optimized *in vitro* culture conditions compared with the *in vivo* conditions, allowing relatively unstable virus particles to survive.

A nucleocapsid must be resistant to environmental degradation yet still be able to disassemble after infection. Disulfide bonds could help with this process by switching between a stable and unstable virus capsid on the basis of different intracellular and extracellular oxidation conditions (12, 30). During the virus life cycle, the disulfide bond strengthens the viral capsid structure and protects the viral genome from oxidative conditions and cellular nucleases when virus particles are formed. Upon infection, the disulfide bond may be cleaved under cytoplasmic reducing conditions, thereby releasing the viral genome into the cell for replication. HCV may utilize the core protein disulfide bond in this way as HCV enters the host cell via clathrin-mediated endocytosis (5) into a low-pH, endosomal compartment (25, 52); this is presumably followed by endosomal membrane fusion and release of the viral capsid into the cytoplasm (38).

Treatment of HCV infection with pegylated interferon in combination with ribavirin is not effective for all patients. Recently, drugs targeting viral proteins NS3/4A and NS5B have been examined in clinical trials. Although these drugs are relatively specific, resulting in fewer side effects and potent antiviral activity, monotherapy can be complicated by rapidly emerging resistant variants carrying mutations that reduce drug efficacy, perhaps due to conformational changes in the target (23, 48, 51). Therefore, viral proteins that are highly conserved among strains and those characterized by low mutation rates may be better targets for drug development. Because the core protein is the most conserved HCV protein and Cys128 is conserved among almost all HCV strains examined, drugs that interact with Cys128 and/or the region around or near this residue will likely show broad-spectrum efficacy to block stable infectious particle formation. Structural analysis of dbd-core should aid with the development of new STAT-Cs that target Cys128 by direct interaction with the sulfide group and/or region around this residue. Until now and still, the mechanism of disulfide bond formation of the core protein on the ER is unknown. Dimerization of the capsid protein by disulfide bond has been reported in some enveloped viruses (9, 19, 54, 56), although some were shown not to be important for virus particle formation (26, 55). Unlike vaccinia virus (46), no redox system of its own has been reported for these viruses. Therefore, further investigations addressing the mechanisms underlying dbd-core formation on the ER may reveal a new mechanism for disulfide bond formation of viral proteins in infected cells.

ACKNOWLEDGMENTS

This work was supported by grants-in-aid from the Ministry of Health, Labor, and Welfare of Japan and by grants-in-aid from the Japan Health Sciences Foundation.

REFERENCES

1. **Abid, K., V. Pazienza, A. de Gottardi, L. Rubbia-Brandt, B. Conne, P. Pugnale, C. Rossi, A. Mangia, and F. Negro.** 2005. An in vitro model of hepatitis C virus genotype 3a-associated triglycerides accumulation. J. Hepatol. **42:**744–751.
2. **Aly, H. H., Y. Qi, K. Atsuzawa, N. Usuda, Y. Takada, M. Mizokami, K. Shimotohno, and M. Hijikata.** 2009. Strain-dependent viral dynamics and virus-cell interactions in a novel in vitro system supporting the life cycle of blood-borne hepatitis C virus. Hepatology **50:**689–696.
3. **Asselah, T., Y. Benhamou, and P. Marcellin.** 2009. Protease and polymerase inhibitors for the treatment of hepatitis C. Liver Int. **29**(Suppl. 1)**:**57–67.
4. **Baron, M. D., and K. Forsell.** 1991. Oligomerization of the structural proteins of rubella virus. Virology **185:**811–819.
5. **Blanchard, E., S. Belouzard, L. Goueslain, T. Wakita, J. Dubuisson, C. Wychowski, and Y. Rouille.** 2006. Hepatitis C virus entry depends on clathrin-mediated endocytosis. J. Virol. **80:**6964–6972.
6. **Boulant, S., M. W. Douglas, L. Moody, A. Budkowska, P. Targett-Adams, and J. McLauchlan.** 2008. Hepatitis C virus core protein induces lipid droplet redistribution in a microtubule- and dynein-dependent manner. Traffic **9:**1268–1282.
7. **Boulant, S., R. Montserret, R. G. Hope, M. Ratinier, P. Targett-Adams, J. P. Lavergne, F. Penin, and J. McLauchlan.** 2006. Structural determinants that target the hepatitis C virus core protein to lipid droplets. J. Biol. Chem. **281:**22236–22247.
8. **Boulant, S., C. Vanbelle, C. Ebel, F. Penin, and J. P. Lavergne.** 2005. Hepatitis C virus core protein is a dimeric alpha-helical protein exhibiting membrane protein features. J. Virol. **79:**11353–11365.
9. **Cornillez-Ty, C. T., and D. W. Lazinski.** 2003. Determination of the multimerization state of the hepatitis delta virus antigens in vivo. J. Virol. **77:**10314–10326.
10. **Dustin, L. B., and C. M. Rice.** 2007. Flying under the radar: the immunobiology of hepatitis C. Annu. Rev. Immunol. **25:**71–99.
11. **Duvignaud, J. B., C. Savard, R. Fromentin, N. Majeau, D. Leclerc, and S. M. Gagne.** 2009. Structure and dynamics of the N-terminal half of hepatitis C virus core protein: an intrinsically unstructured protein. Biochem. Biophys. Res. Commun. **378:**27–31.
12. **Freedman, R. B., B. E. Brockway, and N. Lambert.** 1984. Protein disulphide-isomerase and the formation of native disulphide bonds. Biochem. Soc. Trans. **12:**929–932.
13. **Giannini, C., and C. Brechot.** 2003. Hepatitis C virus biology. Cell Death Differ. **10**(Suppl. 1)**:**S27–S38.
14. **Grakoui, A., C. Wychowski, C. Lin, S. M. Feinstone, and C. M. Rice.** 1993. Expression and identification of hepatitis C virus polyprotein cleavage products. J. Virol. **67:**1385–1395.
15. **Higashi, Y., H. Itabe, H. Fukase, M. Mori, Y. Fujimoto, R. Sato, T. Imanaka, and T. Takano.** 2002. Distribution of microsomal triglyceride transfer protein within sub-endoplasmic reticulum regions in human hepatoma cells. Biochim. Biophys. Acta **1581:**127–136.
16. **Hijikata, M., N. Kato, Y. Ootsuyama, M. Nakagawa, and K. Shimotohno.** 1991. Gene mapping of the putative structural region of the hepatitis C virus genome by in vitro processing analysis. Proc. Natl. Acad. Sci. U. S. A. **88:**5547–5551.
17. **Hijikata, M., H. Mizushima, Y. Tanji, Y. Komoda, Y. Hirowatari, T. Akagi, N. Kato, K. Kimura, and K. Shimotohno.** 1993. Proteolytic processing and membrane association of putative nonstructural proteins of hepatitis C virus. Proc. Natl. Acad. Sci. U. S. A. **90:**10773–10777.
18. **Hope, R. G., and J. McLauchlan.** 2000. Sequence motifs required for lipid droplet association and protein stability are unique to the hepatitis C virus core protein. J. Gen. Virol. **81:**1913–1925.
19. **Hu, H. M., K. N. Shih, and S. J. Lo.** 1996. Disulfide bond formation of the in vitro-translated large antigen of hepatitis D virus. J. Virol. Methods **60:**39–46.
20. **Ishida, S., M. Kaito, M. Kohara, K. Tsukiyama-Kohora, N. Fujita, J. Ikoma, Y. Adachi, and S. Watanabe.** 2001. Hepatitis C virus core particle detected by immunoelectron microscopy and optical rotation technique. Hepatol. Res. **20:**335–347.
21. **Jeng, K. S., C. P. Hu, and C. M. Chang.** 1991. Differential formation of disulfide linkages in the core antigen of extracellular and intracellular hepatitis B virus core particles. J. Virol. **65:**3924–3927.
22. **Kato, N., M. Hijikata, Y. Ootsuyama, M. Nakagawa, S. Ohkoshi, T. Sug-**

imura, and K. Shimotohno. 1990. Molecular cloning of the human hepatitis C virus genome from Japanese patients with non-A, non-B hepatitis. Proc. Natl. Acad. Sci. U. S. A. **87:**9524–9528.
23. **Kieffer, T. L., A. D. Kwong, and G. R. Picchio.** 2010. Viral resistance to specifically targeted antiviral therapies for hepatitis C (STAT-Cs). J. Antimicrob. Chemother. **65:**202–212.
24. **Kim, M., Y. Ha, and H. J. Park.** 2006. Structural requirements for assembly and homotypic interactions of the hepatitis C virus core protein. Virus Res. **122:**137–143.
25. **Koutsoudakis, G., A. Kaul, E. Steinmann, S. Kallis, V. Lohmann, T. Pietschmann, and R. Bartenschlager.** 2006. Characterization of the early steps of hepatitis C virus infection by using luciferase reporter viruses. J. Virol. **80:**5308–5320.
26. **Lee, J. Y., D. Hwang, and S. Gillam.** 1996. Dimerization of rubella virus capsid protein is not required for virus particle formation. Virology **216:**223–227.
27. **Li, M., P. Beard, P. A. Estes, M. K. Lyon, and R. L. Garcea.** 1998. Intercapsomeric disulfide bonds in papillomavirus assembly and disassembly. J. Virol. **72:**2160–2167.
28. **Li, P. P., A. Nakanishi, S. W. Clark, and H. Kasamatsu.** 2002. Formation of transitory intrachain and interchain disulfide bonds accompanies the folding and oligomerization of simian virus 40 Vp1 in the cytoplasm. Proc. Natl. Acad. Sci. U. S. A. **99:**1353–1358.
29. **Liang, T. J., L. J. Jeffers, K. R. Reddy, M. De Medina, I. T. Parker, H. Cheinquer, V. Idrovo, A. Rabassa, and E. R. Schiff.** 1993. Viral pathogenesis of hepatocellular carcinoma in the United States. Hepatology **18:**1326–1333.
30. **Liljas, L.** 1999. Virus assembly. Curr. Opin. Struct. Biol. **9:**129–134.
31. **Majeau, N., R. Fromentin, C. Savard, M. Duval, M. J. Tremblay, and D. Leclerc.** 2009. Palmitoylation of hepatitis C virus core protein is important for virion production. J. Biol. Chem. **284:**33915–33925.
32. **Matsumoto, M., S. B. Hwang, K. S. Jeng, N. Zhu, and M. M. Lai.** 1996. Homotypic interaction and multimerization of hepatitis C virus core protein. Virology **218:**43–51.
33. **McLauchlan, J.** 2000. Properties of the hepatitis C virus core protein: a structural protein that modulates cellular processes. J. Viral Hepat. **7:**2–14.
34. **McLauchlan, J., M. K. Lemberg, G. Hope, and B. Martoglio.** 2002. Intramembrane proteolysis promotes trafficking of hepatitis C virus core protein to lipid droplets. EMBO J. **21:**3980–3988.
35. **Menez, R., M. Bossus, B. H. Muller, G. Sibai, P. Dalbon, F. Ducancel, C. Jolivet-Reynaud, and E. A. Stura.** 2003. Crystal structure of a hydrophobic immunodominant antigenic site on hepatitis C virus core protein complexed to monoclonal antibody 19D9D6. J. Immunol. **170:**1917–1924.
36. **Miyanari, Y., K. Atsuzawa, N. Usuda, K. Watashi, T. Hishiki, M. Zayas, R. Bartenschlager, T. Wakita, M. Hijikata, and K. Shimotohno.** 2007. The lipid droplet is an important organelle for hepatitis C virus production. Nat. Cell Biol. **9:**1089–1097.
37. **Moradpour, D., C. Englert, T. Wakita, and J. R. Wands.** 1996. Characterization of cell lines allowing tightly regulated expression of hepatitis C virus core protein. Virology **222:**51–63.
38. **Moradpour, D., F. Penin, and C. M. Rice.** 2007. Replication of hepatitis C virus. Nat. Rev. Microbiol. **5:**453–463.
39. **Murray, C. L., C. T. Jones, J. Tassello, and C. M. Rice.** 2007. Alanine scanning of the hepatitis C virus core protein reveals numerous residues essential for production of infectious virus. J. Virol. **81:**10220–10231.
40. **Nolandt, O., V. Kern, H. Muller, E. Pfaff, L. Theilmann, R. Welker, and H. G. Krausslich.** 1997. Analysis of hepatitis C virus core protein interaction domains. J. Gen. Virol. **78**(Pt 6)**:**1331–1340.
41. **Okamoto, K., Y. Mori, Y. Komoda, T. Okamoto, M. Okochi, M. Takeda, T. Suzuki, K. Moriishi, and Y. Matsuura.** 2008. Intramembrane processing by signal peptide peptidase regulates the membrane localization of hepatitis C virus core protein and viral propagation. J. Virol. **82:**8349–8361.
42. **Sabile, A., G. Perlemuter, F. Bono, K. Kohara, F. Demaugre, M. Kohara, Y. Matsuura, T. Miyamura, C. Brechot, and G. Barba.** 1999. Hepatitis C virus core protein binds to apolipoprotein AII and its secretion is modulated by fibrates. Hepatology **30:**1064–1076.
43. **Santolini, E., G. Migliaccio, and N. La Monica.** 1994. Biosynthesis and biochemical properties of the hepatitis C virus core protein. J. Virol. **68:**3631–3641.
44. **Seeff, L. B., and J. H. Hoofnagle.** 2003. Appendix: The National Institutes of Health Consensus Development Conference Management of Hepatitis C 2002. Clin. Liver Dis. **7:**261–287.
45. **Sekine-Osajima, Y., N. Sakamoto, K. Mishima, M. Nakagawa, Y. Itsui, M. Tasaka, Y. Nishimura-Sakurai, C. H. Chen, T. Kanai, K. Tsuchiya, T. Wakita, N. Enomoto, and M. Watanabe.** 2008. Development of plaque assays for hepatitis C virus-JFH1 strain and isolation of mutants with enhanced cytopathogenicity and replication capacity. Virology **371:**71–85.
46. **Senkevich, T. G., C. L. White, E. V. Koonin, and B. Moss.** 2000. A viral member of the ERV1/ALR protein family participates in a cytoplasmic pathway of disulfide bond formation. Proc. Natl. Acad. Sci. U. S. A. **97:**12068–12073.
47. **Shavinskaya, A., S. Boulant, F. Penin, J. McLauchlan, and R. Bartenschlager.** 2007. The lipid droplet binding domain of hepatitis C virus core protein is a major determinant for efficient virus assembly. J. Biol. Chem. **282:**37158–37169.
48. **Shimakami, T., R. E. Lanford, and S. M. Lemon.** 2009. Hepatitis C: recent successes and continuing challenges in the development of improved treatment modalities. Curr. Opin. Pharmacol. **9:**537–544.
49. **Tellinghuisen, T. L., M. J. Evans, T. von Hahn, S. You, and C. M. Rice.** 2007. Studying hepatitis C virus: making the best of a bad virus. J. Virol. **81:**8853–8867.
50. **Tellinghuisen, T. L., and C. M. Rice.** 2002. Interaction between hepatitis C virus proteins and host cell factors. Curr. Opin. Microbiol. **5:**419–427.
51. **Thompson, A. J., and J. G. McHutchison.** 2009. Antiviral resistance and specifically targeted therapy for HCV (STAT-C). J. Viral Hepat. **16:**377–387.
52. **Tscherne, D. M., C. T. Jones, M. J. Evans, B. D. Lindenbach, J. A. McKeating, and C. M. Rice.** 2006. Time- and temperature-dependent activation of hepatitis C virus for low-pH-triggered entry. J. Virol. **80:**1734–1741.
53. **Wakita, T., T. Pietschmann, T. Kato, T. Date, M. Miyamoto, Z. Zhao, K. Murthy, A. Habermann, H. G. Krausslich, M. Mizokami, R. Bartenschlager, and T. J. Liang.** 2005. Production of infectious hepatitis C virus in tissue culture from a cloned viral genome. Nat. Med. **11:**791–796.
54. **Wootton, S. K., and D. Yoo.** 2003. Homo-oligomerization of the porcine reproductive and respiratory syndrome virus nucleocapsid protein and the role of disulfide linkages. J. Virol. **77:**4546–4557.
55. **Zhou, S., and D. N. Standring.** 1992. Cys residues of the hepatitis B virus capsid protein are not essential for the assembly of viral core particles but can influence their stability. J. Virol. **66:**5393–5398.
56. **Zhou, S., and D. N. Standring.** 1992. Hepatitis B virus capsid particles are assembled from core-protein dimer precursors. Proc. Natl. Acad. Sci. U. S. A. **89:**10046–10050.
57. **Zweig, M., C. J. Heilman, Jr., and B. Hampar.** 1979. Identification of disulfide-linked protein complexes in the nucleocapsids of herpes simplex virus type 2. Virology **94:**442–450.

MAJOR ARTICLE

Hepatitis B Virus Replication Could Enhance Regulatory T Cell Activity by Producing Soluble Heat Shock Protein 60 From Hepatocytes

Yasuteru Kondo,[1] Yoshiyuki Ueno,[1] Koju Kobayashi,[2] Eiji Kakazu,[1] Masaaki Shiina,[1] Jun Inoue,[1] Keiichi Tamai,[1] Yuta Wakui,[1] Yasuhito Tanaka,[5] Masashi Ninomiya,[1] Noriyuki Obara,[1] Koji Fukushima,[1] Motoyasu Ishii,[3] Tomoo Kobayashi,[4] Hirofumi Niitsuma,[1] Satonori Kon,[2] and Tooru Shimosegawa[1]

[1]Division of Gastroenterology, Tohoku University Hospital, [2]School of Health Science, Tohoku University, [3]Department of Gastroenterology, Miyagi Social Insurance Hospital, and [4]Department of Gastroenterology, Tohoku Rosai Hospital, Sendai, and [5]Clinical Molecular Informative Medicine, Nagoya City University, Nagoya, Japan

Background. HBcAg-specific regulatory T (T_{reg}) cells play an important role in the pathogenesis of chronic hepatitis B. Soluble heat shock proteins, especially soluble heat shock protein 60 (sHSP60), could affect the function of T_{reg} cells via Toll-like receptor.

Methods. We analyzed the relationship between soluble heat shock protein production and hepatitis B virus (HBV) replication with both clinical samples from HBeAg-positive patients with chronic hepatitis B ($n = 24$) and HBeAb-positive patients with chronic hepatitis B ($n = 24$) and in vitro HBV-replicating hepatocytes. Thereafter, we examined the biological effects of sHSP60 with isolated T_{reg} cells.

Results. The serum levels of sHSP60 in patients with chronic hepatitis B were statistically significantly higher than those in patients with chronic hepatitis C ($P < .01$), and the levels of sHSP60 were correlated with the HBV DNA levels ($R = 0.532$; $P < .001$) but not with the alanine aminotransferase levels. Moreover, the levels of sHSP60 in HBV-replicating HepG2 cells were statistically significantly higher than those in control HepG2 cells. Preincubation of $CD4^+$ $CD25^+$ cells with recombinant HSP60 (1 ng/mL) statistically significantly increased the frequency of HBcAg-specific interleukin 10–secreting T_{reg} cells. The frequency of $IL7R^-CD4^+CD25^+$ cells, the expression of Toll-like receptor 2, and the suppressive function of T_{reg} cells had declined during entecavir treatment.

Conclusion. The function of HBcAg-specific T_{reg} cells was enhanced by sHSP60 produced from HBV-infected hepatocytes. Entecavir treatment suppressed the frequency and function of T_{reg} cells; this might contribute to the persistence of HBV infection.

Hepatitis B virus (HBV) is a noncytopathic DNA virus that causes chronic hepatitis and hepatocellular carcinoma as well as acute hepatitis and fulminant hepatitis [1]. HBV now affects more than 400 million people worldwide [2], and persistent infection develops in ~5% of adults and 95% of neonates who become infected with HBV.

It has been shown that the cellular immune system, including cytotoxic T lymphocytes, $CD4^+$ T helper 1 cells, and $CD4^+C25^+FoxP3^+$ regulatory T (T_{reg}) cells, plays a central role in the control of viral infection [3–6]. The hyporesponsiveness of HBV-specific T helper 1 cells and the excessive regulatory function of T_{reg} cells in peripheral blood in patients with chronic hepatitis B has been shown elsewhere [7–10]. Lamivudine treatment of chronic hepatitis B has been reported to restore both $CD4^+$ T cells and cytotoxic T lymphocyte hyporesponsiveness following the decrease of serum levels of HBV DNA and HBV-derived Ag [8, 11–13]. In our previous study, we observed that HBcAg-specific interleukin 10 (IL-10)–secreting T_{reg} cells could play an important role in the immunopathogenesis of chronic hepatitis B [9].

Received 14 July 2009; accepted 3 February 2010; electronically published 9 June 2010.

Potential conflicts of interest: none reported.

Financial support: Ministry of Health, Labor, and Welfare of Japan (Health and Labor Sciences Research Grants for the Research on Measures for Intractable Diseases); Ministry of Education, Culture, Sports, Science, and Technology of Japan (grant 21790642 to Y.K.).

Reprints or correspondence: Yoshiyuki Ueno, Division of Gastroenterology, Tohoku University Graduate School of Medicine, Seiryo 1-1, Aobaku, Sendai, 980-8574, Japan (yueno@mail.tains.tohoku.ac.jp).

The Journal of Infectious Diseases 2010;202(2):202–213

0022-1899/2010/20202-0004$15.00
DOI: 10.1086/653496

Table 1. Clinical Characteristics of Patients with Chronic Hepatitis B or Chronic Hepatitis C Included in This Study

Characteristic	Patients with chronic hepatitis B		Patients with chronic hepatitis C
	HBeAg-positive, HBeAb-negative patients	HBeAg-negative, HBeAb-positive patients	
Age, years	45.16 (12.46)	48.21 (10.23)	48.63 (7.96)
Sex, no. of patients			
Male	12	12	12
Female	12	12	12
ALT level, IU/L	76.91 (39.82)	75.96 (45.90)	76.21 (33.77)
HBV DNA level, log copies/mL	7.83 (0.86)	6.00 (0.81)	NA
Genotype, % of patients			
A	0	4.17	NA
B	12.5	8.33	NA
C	87.5	87.5	NA

NOTE. Data are mean values (standard deviations), unless otherwise indicated. ALT, alanine aminotransferase; HBV, hepatitis B virus; NA, not applicable.

Many research groups have reported the possible induction of anergy by T_{reg} cells, which constitutively express CD25 (the interleukin 2 receptor α chain) in the physiological state [14–16]. In humans, this population of T_{reg} cells, as defined by $CD4^+CD25^+CTLA4^+$ cells, $CD4^+CD25^+FoxP3^+$ cells, or $CD4^+CD25^+IL7R^-$ cells, constitutes 5%–10% of peripheral $CD4^+$ T cells and has a broad repertoire that recognizes various self and nonself antigens. It has been reported that T_{reg} cells have several different mechanisms in suppressing various kinds of immune cells [17, 18]. The important mechanisms are cell to cell contact and secretion of cytokines including IL-10 and transforming growth factor β (TGF-β) [19, 20]. HBcAg derived from HBV might induce T_{reg} cells to escape from immunological pressure, as reported in persistent infection with Epstein-Barr virus, hepatitis C virus (HCV), and human immunodeficiency virus type 1 [21–23]. Some results have indicated that reduction of HBV replication could reduce the frequency and/or function of T_{reg} cells in patients with chronic hepatitis B [4, 5, 8]. However, the key factors that affect HBcAg-specific T_{reg} cells in the replication of HBV remain unclear.

The mammalian 60-kDa heat shock protein is a many-faceted molecule. In addition to serving as a chaperone, heat shock protein 60 (HSP60) is expressed by different types of cells following their exposure to stress or immune responses and is present in the blood during inflammation [24–27]. Recently, HSP60 was reported to enhance the function of $CD4^+CD25^+$ regulatory T cell function via Toll-like receptor 2 (TLR2) signaling [28].

In this study, we investigated the serum level of HSP60 in patients with chronic hepatitis B and the relevance of HBcAg-specific IL-10-secreting T_{reg} cells and HSP60. We report evidence of the production of soluble HSP60 (sHSP60) from HBV-replicating hepatocytes, by use of clinical samples from patients with chronic hepatitis B and an in vitro HBV replication system. In addition, reductions of $CD4^+CD25^+IL7R^-$ T_{reg} cells and TLR2 expression on T_{reg} cells were observed during entecavir therapy. This study could contribute to better understanding of the immunopathogenesis of chronic hepatitis B and the development of immune-based treatment.

MATERIALS AND METHODS

Patients. Forty-eight patients with chronic hepatitis B were enrolled in this study (Table 1). The patients had serum levels of HBV DNA of >5.0 log copies/mL and had elevated alanine aminotransferase (ALT) levels (reference range, <40 IU/L) for >6 months prior to the study. To focus the analysis on the active phase of chronic hepatitis B, we excluded asymptomatic carriers and patients with immune tolerance by age (<30 years old), ALT values (<40 IU/L), and HBV DNA levels (<5.0 log copies/mL). Twenty-four patients were seropositive for HBeAg, and 24 patients were seropositive for anti-HBeAb. None of the patients tested positive for antibodies to hepatitis C virus or had liver disease due to other causes, such as alcohol, drugs, congestive heart failure, and autoimmune disease. Twenty-four patients with chronic hepatitis C and 10 healthy subjects were included as control subjects. Permission for the study was obtained from the Ethics Committee at Tohoku University Graduate School of Medicine (permission no. 2006-194]). Written informed consent was obtained from all the participants enrolled in this study. Participants were monitored for 6 months, and peripheral blood samples were obtained and assessed at 1, 2, 3, and 6 months. At each assessment, patients were evaluated for serum levels of HBV DNA, HBeAg, and anti-HBe, blood chemistry, and hematology. Levels of HBsAg, anti-HBs, total and immunoglobulin anti-HBc, HBeAg, anti-HBe, and anti–

hepatitis C virus were determined by means of commercial enzyme immunoassay kits (Abbott Laboratories). Serum levels of HBV DNA were measured by means of an Amplicor polymerase chain reaction (PCR) assay (lower limit of detection, 2.6 log copies/mL; Roche). High titers of HBV DNA were measured by means of a transcription-mediated amplification-hybridization protection assay (TMA; lower limit of detection, 3.7 log genome equivalents per milliliter). Data were adjusted by means of the following formula: Amplicor value = 0.83 × (TMA value) + 0.67.

Reagents. The following antibodies were used: CD3–allophycocyanin (APC), CD4–peridinin chlorophyll protein complex (PerCP), CD25–fluorescein isothiocyanate (FITC), CD25-phycoerythrin (PE), CD127-PE, Alexa Fluor 488 mouse anti–human CD282 (TLR2), CD284 (Toll-like receptor 4 [TLR4]), and isotype-matched control antibodies purchased from BD Bioscience. Recombinant HBcAg was obtained from Biodesign International. Recombinant HSP60 (rHSP60) was purchased from Stressgen.

Quantification of sHSP60 and soluble heat shock protein 70 (sHSP70) levels. Levels of HSP60 and heat shock protein 70 (HSP70) were quantified by use of HSP60 and HSP70 enzyme-linked immunosorbent assay (ELISA) kits (Stressgen). The serum samples from patients and supernatants from cell cultures were collected at sampling points and stocked at −20°C. The ELISA procedure was performed according to the manufacturer's protocol. First, 100-μL prepared samples were added to wells of anti-HSP60-coated plates. Then the reaction of the anti-HSP60 and horseradish peroxidase conjugate was performed after incubation and washing. Absorbance was measured at 450 nm. The HSP60 sample concentration was calculated by use of a standard curve.

Isolation of peripheral blood mononuclear cells (PBMCs) and T_{reg} cells. PBMCs were isolated from fresh heparinized blood by means of Ficoll-Hypaque density gradient centrifugation. T_{reg} cells were isolated by use of a Dynabeads regulatory $CD4^+CD25^+$ T cell kit (Invitrogen). T_{reg} cells were isolated according to the manufacturer's protocol. In brief, $CD4^+$ cells were isolated from PBMCs by means of negative selection. The remaining cells included the PBMCs depleted of $CD4^+$ cells. Then the $CD4^+CD25^+$ cells were selected positively by use of $CD25^+$ antibody combined with beads. Finally, the beads were detached by means of Detachabead (Invitrogen), because the function of T_{reg} cells might be modified by anti-CD25 antibody.

Coculture of γ-irradiated HBcAg-presenting antigen-presenting cells (APCs) and T_{reg} cells. During the isolation of T_{reg} cells, PBMCs depleted of $CD4^+$ cells could be obtained for use as APCs. PBMCs depleted of $CD4^+$ cells were stimulated at 1×10^6 cells/mL in Roswell Park Memorial Institute 1640 medium containing 10% fetal bovine serum with HBcAg (10 μg/mL) for 12 h at 37°C. Then these γ-irradiated cells were coincubated with 1×10^5 isolated T_{reg} cells that were untreated pretreated with TLR2 and TLR4 neutralizing antibody and rHSP60 (1 ng/mL) (Figures 1*A* and 2).

IL-10 secretion assay. Isolated T_{reg} cells were stimulated with HBcAg-presenting autologous γ-irradiated APCs for 12 h at 37°C. IL-10-secreting cells were stained by adding 10 μL of IL-10-detection antibody (PE-conjugated) together with anti-CD4-PerCP, anti-CD25-FITC, and anti-CD3-APC.

Flow cytometry. PBMCs were stained with CD3-APC, CD4-PerCP, CD25-FITC, and CD127-PE antibodies for 15 min on ice to analyze the frequency of $CD4^+CD25^+IL7R^-$ cells. CD4-PerCP, CD25-PE, and Alexa Fluor 488 mouse anti–human CD282 (TLR2) or CD284 (TLR4) were used for the analysis of TLR2 and TLR4 expression on $CD4^+CD25^+$ cells. Isotype-matched control antibodies were used for adjustment of the fluorescence intensity.

Construction of plasmids. The HBV plasmids was constructed as described elsewhere, with minor modifications [29]. In brief, a serum sample from one of the consecutive patients with fulminant hepatitis B (fulminant hepatitis clone 2), whose serum level of HBV DNA was the highest of the 5 patients, was used to extract total DNA (QIAamp DNA blood mini kit; Qiagen), which was subjected to nested PCR for 2 overlapping fragments; the amplified fragments were nucleotides 1051–3215/1–327 (2492 nucleotides; fragment A) and nucleotides 180–1953 (1774 nucleotides; fragment B). Then the vectors were digested with XbaI, and the XbaI-XbaI site of fragment A-pUC118 was ligated to the XbaI-XbaI site of fragment B-pUC118. Finally, a plasmid containing a 1.3-fold HBV genome (nucleotides 1051–3215/1–1953) was constructed and named pBFH2.

Cell culture and transfection. Human hepatoma HepG2 cells were incubated in Dulbecco modified Eagle medium supplemented with 10% bovine serum at 37°C and 5% carbon dioxide. For the assay of HBV replication, 6-well plates were seeded with 5×10^5 HepG2 or Huh7 cells each. On the next day, 1.5 μg of plasmid DNA were transfected to these cells by use of TransIT LT-1 transfection reagent (Mirus), and the culture supernatant and cells were collected 3 d later. The transfection efficiency was evaluated with a Great EscAPe secreted alkaline phosphatase reporter system 3 (Clontech), in which 10 ng/mL of a reporter plasmid expressing secreted alkaline phosphatase was cotransfected. Experiments were performed at least in triplicate.

Quantification of extracellular HBV DNA, HBsAg, and HBeAg levels. To digest the input plasmid DNA in the culture supernatant, 5 μL of the supernatant was treated with 5 U of DNase I (TaKaRa Bio) at 37°C for 1 h, and the reaction was stopped with edetic acid. Then total DNA was extracted with a QIAamp DNA blood mini kit, and 10 μL of 200-μL DNA solution was subjected to real-time PCR by use of a LightCycler

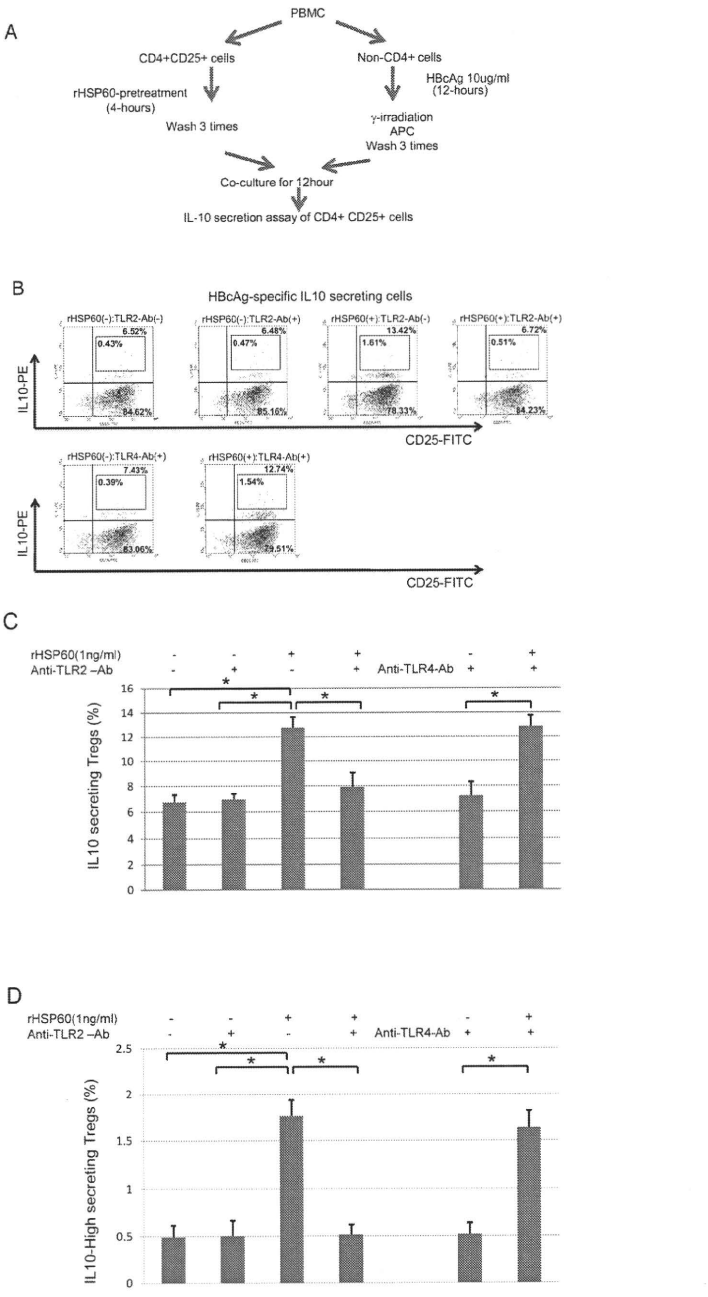

Figure 1. Effects of heat shock protein 60 (HSP60) on HBcAg-specific interleukin 10 (IL-10)–secreting regulatory T (T_{reg}) cells. *A,* Flow chart of the methods. *B,* Representative dot plots of IL-10-secreting cells in the $CD4^+CD25^+$ cells. The mixed cells (antigen-presenting cells [APCs; $CD4^-$] and isolated $CD4^+CD25^+$ cells) were stained with anti-CD4–peridinin chlorophyll protein complex (PerCP), anti-CD25–fluorescein isothiocyanate (FITC), and anti-IL-10-phycoerythrin (PE). The numbers in each top right quadrant indicate the frequencies of $CD25^+$ IL-10-secreting cells among the $CD4^+$ cells. The numbers in each bottom right quadrant indicate the frequencies of $CD4^+CD25^+IL\text{-}10^-$ cells among the $CD4^+$ cells. The numbers in each box in the top right quadrant indicate the frequencies of $CD25^+$ IL-10-secreting cells among the $CD4^+$ cells. *C,* Representative results for a sample from 1 patient with chronic hepatitis B (samples were obtained from 3 patients with chronic hepatitis B; this experiment was repeated 3 times). Bars indicate the percentage of IL-10-secreting cells among the $CD4^+$ cells with various kinds of pretreatment. *D,* Percentage of high–IL-10-secreting cells among the $CD4^+$ cells. Error bars indicate the standard deviation of 3 independent experiments with a sample from 1 patient with chronic hepatitis B. Three independent experiments yielded similar results to those shown in panels *C* and *D*. $^*P < .05$.

This figure is available in its entirety in the online version of the *Journal of Infectious Diseases*.

Figure 2. Effect of recombinant heat shock protein 60 (rHSP60) on the interleukin 10 (IL-10)–secreting activity of $CD4^+CD25^+$ cells.

system (Roche). ELISA kits were used to assay HBsAg (Hope Laboratories) and HBeAg (BioChain Institute) in 50 μL of the culture supernatant.

Sequence analysis of HBV DNA. The presence of HBV DNA in the serum samples was determined by means of PCR, as described elsewhere [30]. Nucleic acids were extracted from 100 mL of serum and subjected to nested PCR for the S gene. The amplification product of the first-round PCR was 461 bp, and that of the second-round PCR was 437 bp. The amplification products were sequenced directly on both strands by use of the BigDye Terminator Cycle Sequencing Ready reaction kit on an ABI Prism 3100 genetic analyzer (Applied Biosystems).

Carboxyfluorescein succinimidyl ester (CFSE) staining and suppression assay. The suppressive activity of regulatory T cells was analyzed by use of a CellTrace CFSE cell proliferation kit (Molecular Probes). Staining methods were followed according to the manufacturer's protocol. Briefly, the collected $CD4^+CD25^-$ cells were washed and resuspended in prewarmed phosphate-buffered saline with 0.1% bovine serum albumin at a final concentration of 3×10^5 cells/mL. CFSE solution (5 μm) was added and incubated at 37°C for 10 min. Stained cells were washed 3 times and incubated with unstained $CD4^+CD25^+$ T_{reg} cells and CD3CD28-coated stimulation beads (T cell expander) for an additional 3 d. The cells were analyzed by means flow cytometry with 488-nm excitation and emission filters.

Statistics. The data in Figures 3, 4, 1*C*, 1*D*, and 5 were analyzed by use of the independent *t* test. Statistical correlation analysis of the data in Figure 6 was performed by use of the Kendall τ_b test. The data in Figure 7 were analyzed by use of the Wilcoxon rank sum test. All of the statistical analyses were performed with SPSS software (version 10.0; SPSS). Results for which $P < .05$ were considered to be statistically significant.

RESULTS

Levels of sHSP60 and sHSP70 in samples from HBeAg-positive patients with chronic hepatitis B, HBeAg-negative patients with chronic hepatitis B, and control patients with chronic hepatitis C. The patients' characteristics, including age, sex, and ALT level, were matched among the different patient groups because the levels of sHSP60 and sHSP70 might be influenced by these factors (Table 1). The mean (± standard deviation [SD]) serum level of sHSP60 was 5.77 ± 1.19 ng/mL in HBeAg-positive patients with chronic hepatitis B, 4.12 ± 1.37 ng/mL in HBeAg-negative patients with chronic hepatitis B, 2.11 ± 0.96 ng/mL in patients with chronic hepatitis C, and 0.54 ± 0.46 ng/mL in healthy subjects. The levels of sHSP60 in patients with chronic hepatitis B (HBeAg-positive and HBeAg-negative) were statistically significantly higher than those in patients with chronic hepatitis C (Figure 3). On the other hand, the mean (± SD) serum level of sHSP70 was 7.89 ± 3.51 ng/mL in HBeAg-positive patients with chronic hepatitis B, 7.73 ± 3.71 ng/mL in HBeAg-negative patients with chronic hepatitis B, 8.09 ± 3.64 ng/mL in patients with chronic hepatitis C, and 3.54 ± 0.46 ng/mL in healthy subjects. There were no statistically significant differences in the level of sHSP70 between the chronic hepatitis B and chronic hepatitis C patient groups (Figure 3). Then we examined the correlations between the HSP60, HSP70, and HBV DNA or ALT levels. The levels of sHSP60 were correlated with the HBV DNA levels ($r = 0.532$; $P < .001$) but not with the ALT levels ($r = 0.101$; $P = .315$) (Figures 6*A* and 6*B*). On the other hand, the levels of sHSP70 were correlated with the ALT levels ($r = 0.520$; $P < .001$) but not with the HBV DNA levels ($r = 0.076$; $P < .449$) (Figure 6*C* and 6*D*).

HBV replication could directly induce sHSP60 production in vitro. Two kinds of plasmids carrying a 1.3-fold HBV genome that could replicate in HepG2 cells were used to analyze whether HBV replication could affect the production of sHSP60 in culture medium. The transfection efficiency was almost the

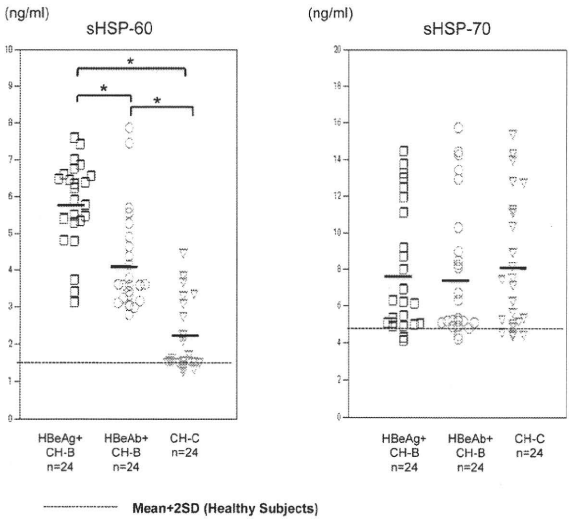

Figure 3. Quantification of serum levels of heat shock protein 60 (HSP60) and heat shock protein 70 (HSP70) in HBeAg-positive patients with chronic hepatitis B (CH-B), HBeAb-positive patients with CH-B, and patients with chronic hepatitis C (CH-C). Serum levels of HSP60 and HSP70 were quantified by means of enzyme-linked immunosorbent assay. The bar represents the means of the levels of HSP60 and HSP70. Dotted lines indicate the mean value plus 2 times the standard deviation (SD) of the levels of healthy subjects.

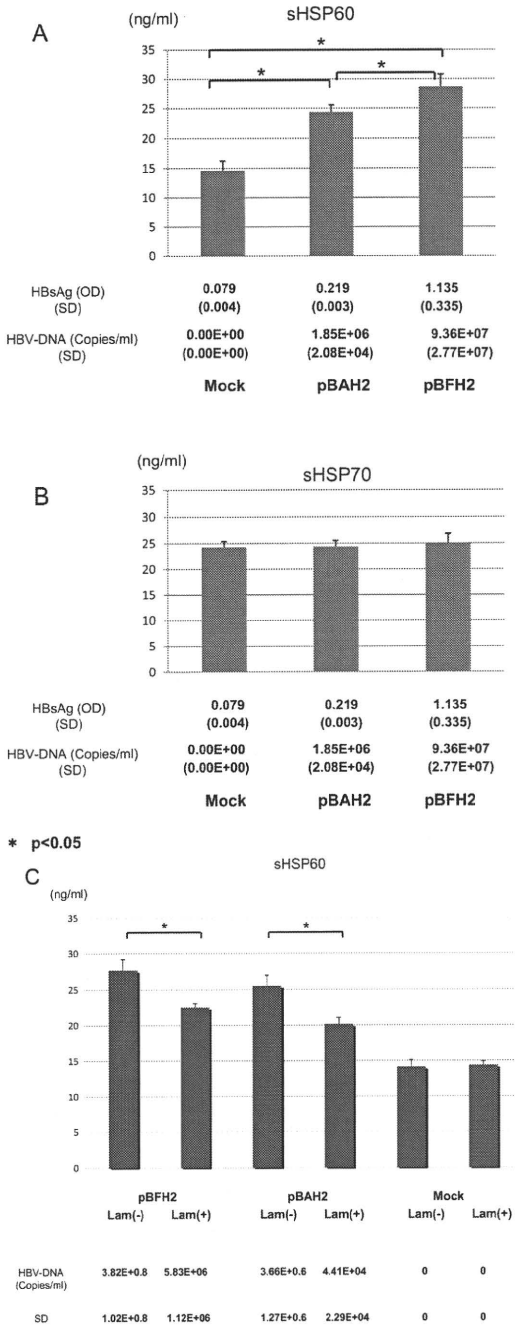

Figure 4. Direct effect of hepatitis B virus (HBV) on the production of heat shock protein 60 (HSP60) and heat shock protein 70 (HSP70). Two kinds of plasmid (pBAH2 and pBFH2) carrying a 1.3-fold HBV genome that could replicate in HepG2 cells and a mock plasmid were used to analyze whether HBV replication affects the production of soluble HSP60 (sHSP60) in culture medium. The levels of sHSP60 and soluble HSP70 (sHSP70) were compared among the 3 plasmid groups. Bars indicate the levels of HSP60 (*A*) and HSP70 (*B*). The HBsAg and HBV DNA levels and standard deviations (SDs) are included below the bar graphs. *C*, Levels of sHSP60 in cells with and those in cells without lamivudine treatment. The cells were treated with lamivudine (Lam; 0.5 μmol/L) for 72 h. Three independent experiments were performed.

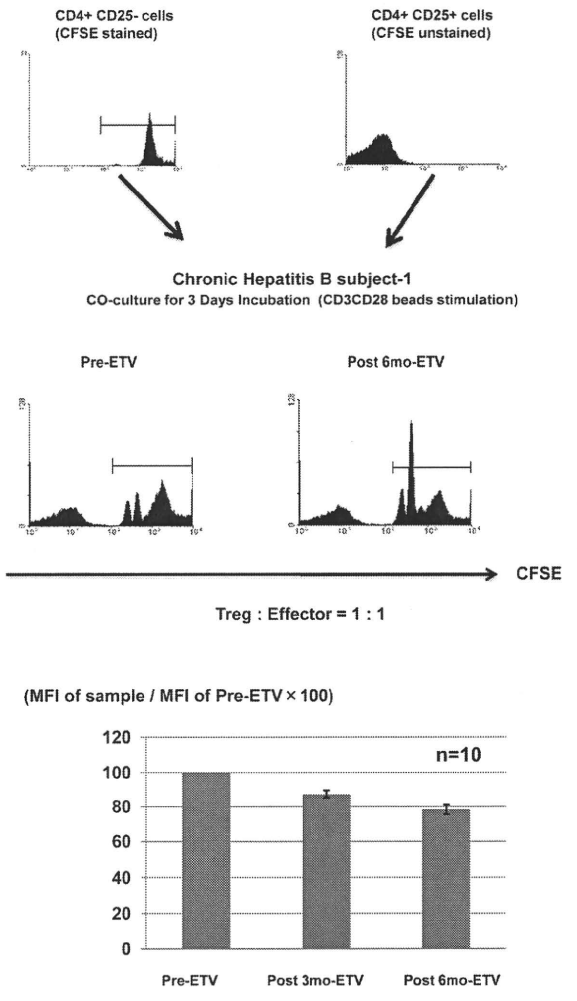

Figure 5. Suppression assay of regulatory T (T_{reg}) cells. The suppressive activity of T_{reg} cells was analyzed by means of coincubation of unstained isolated T_{reg} cells and autologous $CD4^+CD25^-$ cells with carboxyfluorescein succinimidyl ester (CFSE) staining. *A*, Representative histogram of CFSE-stained $CD4^+CD25^-$ effector cells and unstained $CD4^+CD25^+$ T_{reg} cells. *B*, Various levels of cell division in $CD4^+CD25^-$ effector cells observed 3 d after coincubation with CD3CD28-coated beads. *C*, Mean fluorescence intensity (MFI) of CFSE staining of $CD4^+CD25^-$ cells before treatment, 3 months after the start of entecavir (ETV) treatment, and 6 months after the start of entecavir treatment. The bars show the MFI of the samples divided by the MFI of the pretreatment samples ×100. The error bars indicate the standard deviations of the data.

same among the different plasmids (data not shown). The mean (± SD) HBV DNA levels of pBAH2 and pBFH2 were $1.85 \times 10^6 \pm 2.08 \times 10^4$ and $9.36 \times 10^7 \pm 2.77 \times 10^7$ copies/mL, respectively. The levels of sHSP60 in the supernatant of the pBAH2- and pBFH2-transfected HepG2 cells were statistically significantly higher than that of the mock-transfected HepG2 cells ($P < .05$) (Figure 4*A*). However, the levels of sHSP70 in the supernatant of the pBAH2- and pBFH2-transfected HepG2 cells were comparable with that of the mock-transfected HepG2 cells (Figure 4*B*). The addition of HBV-derived antigen in the culture supernatant could not increase the level of sHSP60 (data not shown). We performed the experiment on the suppression of HBV replication by nucleoside analogues in vitro. The suppression of HBV replication could statistically significantly reduce the production of sHSP60 (Figure 4*C*). These data indicate that HBV replication could increase the level of sHSP60 in the supernatant of the hepatocyte culture.

The effect of HSP60 on the HBcAg-specific IL-10-secreting T_{reg} cells. Previously, we found that HBcAg-specific IL-10-secreting cells could play an important role in the hyporesponsiveness of T cells in patients with chronic hepatitis B [9]. The effects of HSP60 on HBcAg-specific IL-10-secreting T_{reg} cells were analyzed. The appropriate dose of rHSP60 pretreatment was determined by use of PBMCs from healthy subjects (Figure 2). Pretreatment with rHSP60 could increase the frequency of HBcAg-specific IL-10-secreting cells statistically significantly ($P < .01$) and enhance the function of IL-10 secretion of HBcAg-specific T_{reg} cells, because the frequencies of high-intensity cells with IL-10 staining in HSP60 pretreatment T_{reg} cells were statistically significantly higher than those of control groups (Figure 1*D*). Moreover, these effects were completely blocked by neutralizing TLR2 antibody but not by TLR4 antibody. These data indicate that HSP60 might enhance the susceptibility and function of IL-10 secretion of HBcAg-specific T_{reg} cells.

Sequential analysis of clinical samples collected during entecavir therapy. Ten patients were selected for sequential analysis during entecavir therapy. The titers of HBV DNA and the ALT level rapidly decreased during entecavir therapy (Figures 7*A* and 7*B*). The serum levels of HSP60 had statistically significantly decreased at 3 months and at 6 months after the start of entecavir therapy. The frequency of T_{reg} cells and the expression level of TLR2 during entecavir treatment were quantified sequentially for up to 6 months during treatment by means of flow cytometry analysis. The frequency of $CD4^+CD25^+$ cells decreased, although not statistically significantly. On the other hand, the frequency of $CD4^+CD25^+IL7R^-$ cells (subpopulation of $CD4^+CD25^+$ cells) had statistically significantly decreased at 3 months and at 6 months after the start of entecavir therapy. The reason for the discrepancy could be that $CD4^+CD25^+$ cells included not only T_{reg} cells but also activated $CD4^+$ effector cells. Previously, some research groups had found that $CD4^+CD25^+FoxP3^+$ cells are almost the same as $CD4^+CD25^+IL7R^-$ cells. Therefore, our data indicate that entecavir therapy could reduce the frequency of T_{reg} cells. We also investigated the frequency of $CD4^+CD25^+FoxP3^+$ cells during lamivudine therapy (Figure 8). The frequency of

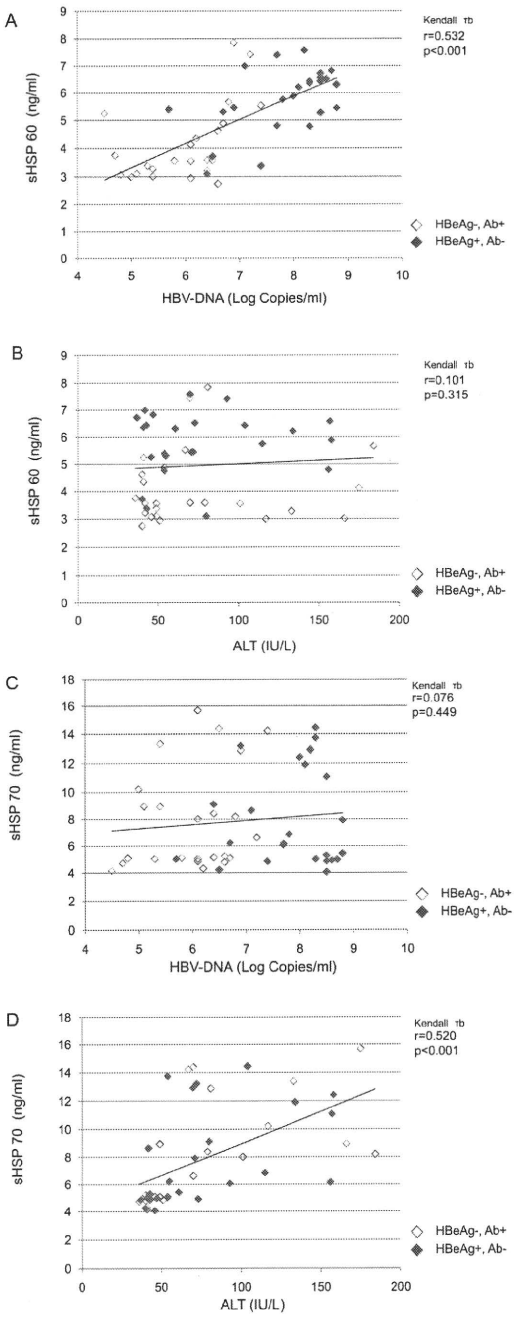

Figure 6. Analysis of the correlations between levels of heat shock proteins (HSPs), hepatitis B virus (HBV) DNA, and alanine aminotransferase (ALT). Open symbols indicate the values in samples from HBeAg-negative, HBeAb-positive patients. Filled symbols indicate the values in samples from HBeAg-positive, HBeAb-negative patients. The statistical analysis was performed by use of nonparametric Kendall τ_b methods. An approximately straight line is included in each graph. *A,* Correlation between heat shock protein 60 (HSP60) level and HBV DNA level. *B,* Correlation between HSP60 level and ALT level. *C,* Correlation between heat shock protein 70 (HSP70) level and HBV DNA level. *D,* Correlation between HSP70 level and ALT level.

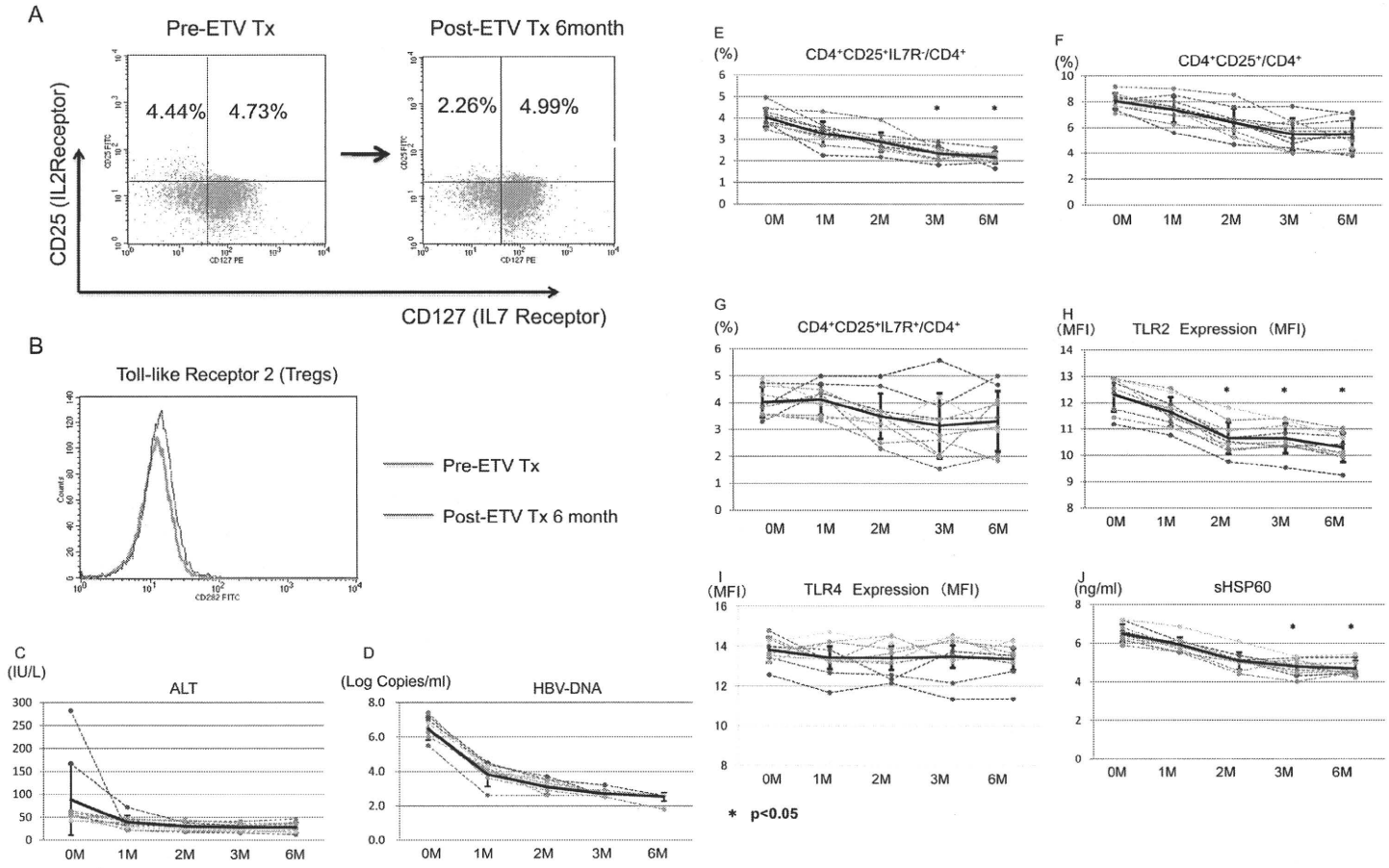

Figure 7. Sequential analysis of primary lymphocytes and soluble heat shock protein 60 (sHSP60) during entecavir (ETV) therapy. *A,* Representative dot plots of the $CD4^+CD25^+IL7R^-$ cells before treatment and 6 months after the start of treatment. Peripheral blood mononuclear cells were stained with anti-CD3, anti-CD4, anti-CD25, and anti–IL7R (CD127). The phenotypes of the $CD4^+$ cells were determined as follows: $CD4^+CD25^+IL7R^-$ cells were identified as regulatory cells and $CD4^+CD25^+IL7R^+$ cells were identified as activated $CD4^+$ cells. *B,* Representative histogram of Toll-like receptor 2 (TLR2) surface expression on $CD4^+CD25^+$ regulatory T (T_{reg}) cells before treatment and 6 months after the start of treatment. *C* and *D,* Serum levels of alanine aminotransferase (ALT) and hepatitis B virus (HBV) DNA during ETV treatment. Solid black lines and error bars indicate the mean values and standard deviations, respectively. *E–G,* Frequencies of $CD4^+CD25^+IL7R^-$cells, $CD4^+CD25^+$ cells, and $CD4^+CD25^+IL7R^+$ cells among $CD4^+$ cells during ETV treatment, respectively. *H* and *I,* Mean fluorescence intensity (MFI) of TLR2 and Toll-like receptor 4 (TLR4) expression on $CD4^+CD25^+$ cells during ETV treatment. *J,* Serum levels of sHSP60 during ETV treatment. $^*P < .01$ for comparison between pretreatment levels and posttreatment levels.